Volume 19 | Number 29 | 7 August 2017 | Pages 4035–4228

CrystEngComm

rsc.li/crystengcomm

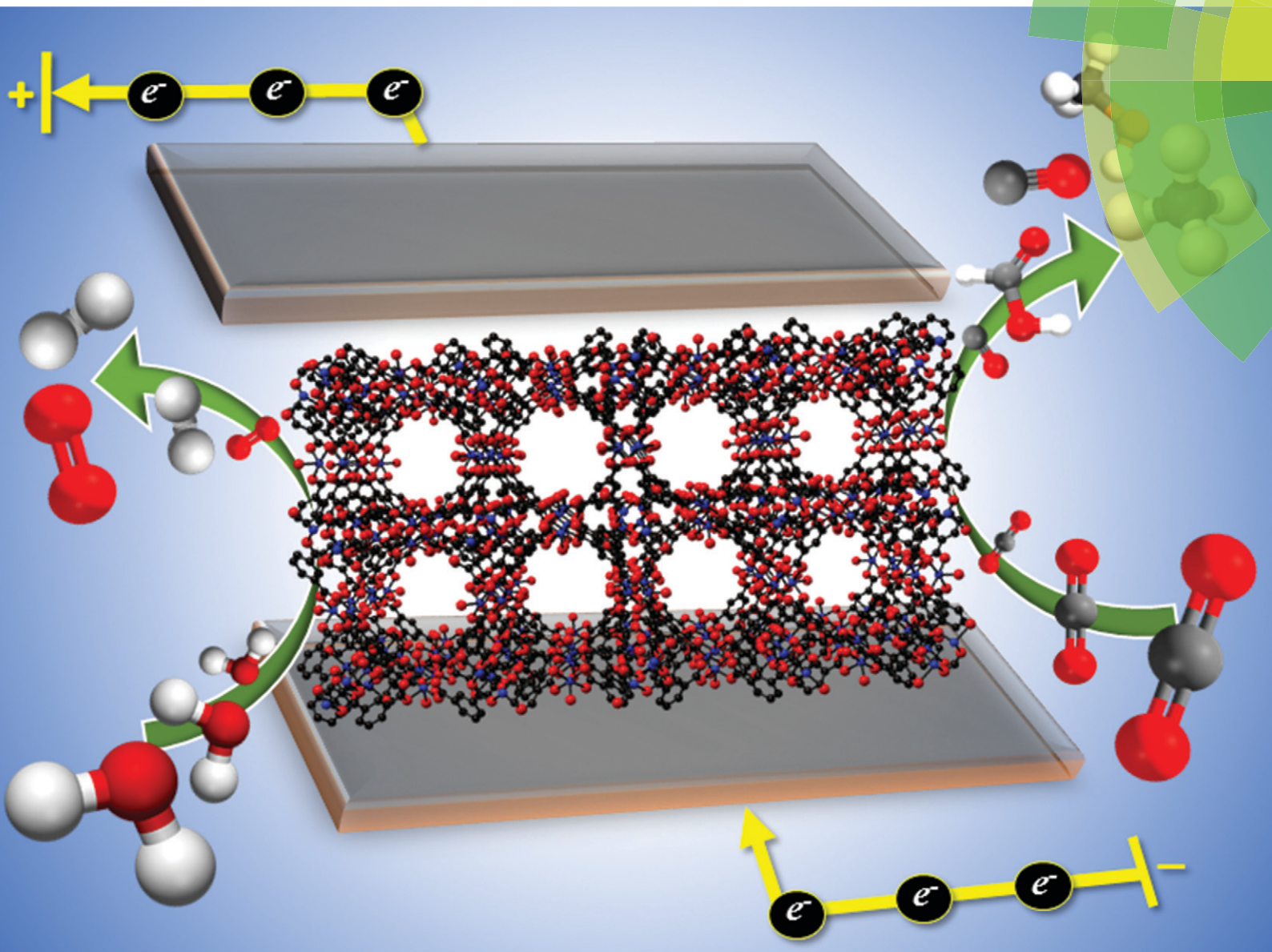

Themed issue: Metal–Organic Framework Catalysis

ROYAL SOCIETY OF CHEMISTRY

HIGHLIGHT
Deanna M. D'Alessandro *et al.*
Perspectives on metal–organic frameworks with intrinsic electrocatalytic activity

CrystEngComm

HIGHLIGHT

View Article Online
View Journal | View Issue

Cite this: *CrystEngComm*, 2017, **19**, 4049

Perspectives on metal–organic frameworks with intrinsic electrocatalytic activity

Marcello B. Solomon,[a] Tamara L. Church[ab] and Deanna M. D'Alessandro*[a]

Received 29th January 2017,
Accepted 6th March 2017

DOI: 10.1039/c7ce00215g

rsc.li/crystengcomm

This highlight article focuses on the rapidly emerging area of electrocatalytic metal–organic frameworks (MOFs) with a particular emphasis on those systems displaying *intrinsic* activity. Three electrocatalytic conversion processes are discussed, including CO_2 reduction, the hydrogen evolution reaction (HER) and the oxygen evolution reaction (OER), as well as a selection of other relevant examples. The scope of our discussion encompasses aspects of MOF structure that are key to their function, performance characteristics such as stability and selectivity, together with methods for interfacing MOFs with surfaces. Key challenges that have emerged are highlighted in addition to opportunities that are relevant to the field in the design of more stable, selective and robust electrocatalysts for a range of industrial processes.

1. Introduction

The demand for energy to satisfy the needs of an ever-growing population has led to the reliance on fossil fuels for their high energy density to generate the necessary power for the human population. Industrialisation has been heavily dependent on the use of coal, which is responsible for over 40% of electricity production worldwide.[1] Additionally, in excess of 12 million tonnes of oil and 8 million cubic tonnes of natural gas are consumed daily to provide energy. The dependence on fossil fuels has led to the increased concentration of CO_2 into the atmosphere, with CO_2 levels surpassing 400 ppm for the first time in recorded history.[2] Efforts to reduce the reliance on fossil fuels for the production of energy has seen various approaches. One such strategy is CO_2 capture and conversion, to reduce the levels of CO_2 in the atmosphere (the subject of many recent reviews[2–9]), and to capitalise on the rich carbon source that CO_2 can provide as a chemical feedstock. Another strategy is the use of renewable energy sources such as wind, hydro and solar-based energies to generate more environmentally benign fuels such as H_2 and O_2 in renewable fuel cells.

Studies into the feasibility of cheap and abundant feedstocks, such as CO_2 and H_2O, have probed their uses as alternatives to fossil fuels. The benefit of CO_2 being a cheap and abundant source of carbon is limited by carbon being in its most oxidised form; this means that it is difficult to chemically access for transformation into a commodity chemical. Investing energy to convert CO_2 into a more reactive intermediate could enable the generation of a cleaner fuel source. The conversion of H_2O can generate both H_2 and O_2 which supports the move towards a hydrogen fuel economy.[10] The challenge here lies in the limitations of conventional methods for water splitting, including the use of high temperatures or pressures, resulting in a lower efficiency of H_2 production. As a consequence, catalysts are required to lower the energy penalty associated with these reaction pathways and provide more viable routes for conversion.

Currently, there exist a number of classes of catalysis for the generation of useful fuels. These include, but are not limited to biocatalysis,[11] chemical catalysis (including organometallic[12] and organocatalysis[13]), photocatalysis[14] and electrocatalysis.[15] A particular attraction of electrocatalysis lies in its relative simplicity and the ability to control the reaction through modulation of electric potential difference. Unlike biocatalysis, the electrocatalytic conversion does not require the additional complexity of modelling enzyme stability (which is highly pH dependent) and metabolic pathways for multi-step biocatalytic reactions.[11] Electrocatalysts are considered a feasible alternative to organometallic catalysts since a large proportion of the latter are based on rare and precious metals, are tedious to manipulate due to their traditionally air sensitive nature and may contribute to heavy metal pollution upon their use. While the limitations in cost, robustness and abundance of precursors for organometallic catalysis can be addressed by designing organocatalysts, they require a high catalyst loading to achieve catalytic transformation in high efficiencies.[16] Finally, although photocatalytic catalysis in many cases (*e.g.*, CO_2 reduction) may allow for a more direct conversion of a substrate to a product, the conversion measured by quantum yield is often very low.[17] In comparison,

[a] *School of Chemistry, The University of Sydney, New South Wales, 2006, Australia. E-mail: deanna.dalessandro@sydney.edu.au*
[b] *Department of Materials and Environmental Chemistry, Stockholms Universitet, 106 91, Sweden*

some electrocatalytic transformations can occur in Faradaic efficiencies of up to 100%.[18] Electrocatalysis is also beneficial since it is relatively easily coupled with a renewable energy source such as hydro, solar or wind power to generate the necessary potential for conversion.[19]

Techniques in electrocatalysis were initially developed in the solution phase because it is comparatively simple to apply solution state spectroscopic techniques to quantify products of catalytic transformation, understand the kinetics of the reaction and elucidate the mechanism.[20,21] It is also more straightforward to generate a library of discrete compounds for solution state electrochemistry in order to systematically modulate the catalyst and relate its structure to its electrochemical function. Homogeneous electrocatalysis has been very well developed and is the subject of many reviews for applications in CO_2 conversion,[20,22] H_2 production,[23–27] O_2 production,[28–30] general organic synthesis[31] and for industrial applications;[32,33] however, with the increasing number of electroactive solid-state materials being reported in the literature,[34] alternative methods for assessing catalysts and quantifying catalytic processes need to be explored.

Despite the advantages of homogeneous catalysis (tunability and chemical robustness), heterogeneous catalysts possess a number of long-term benefits in the context of electrocatalysis. Homogeneous electrocatalysts are only electroactive at the surface of an electrode, or within the diffuse double layers of an electrochemical cell, such that bulk electrocatalysis is dictated by diffusion and mass transport.[35] In solution, electroactive complexes may physically or chemically interact with each other, triggering a deactivation process of the active site.[36] By suspending a discrete complex in a crystalline matrix, it may be possible to control the environment of the catalytically active site to avoid its deactivation and lengthen its lifetime.[37] The use of a heterogeneous catalyst may also open up the possibility of using solvents that are more favourable for electrochemistry, since solubility is not a requirement for heterogeneous catalyst function.[38] If a heterogeneous scaffold is localised on an electrode, it will not be controlled by the rate of diffusion in the solvent. Heterogenisation also prevents the two active half-cell reactions in an electrochemical cell from interfering with each other. For example, if an active homogeneous reduction catalyst reaches the anode, then it may partake in the oxidation half reaction of the electrochemical cell, or may itself undergo oxidative degradation.[39] Improving the conductivity of a crystalline matrix containing catalytically active sites may allow for charge propagation through the solid, leading to improved overall rates of catalysis. With constant improvements in solid state spectroscopic and electrochemical techniques, and the development of new experimental methods to study surfaces, heterogeneous catalysis is no longer limited by restrictions such as low temperatures and high vacuum conditions[40] or inhomogeneous surfaces.[41] Finally, heterogeneous catalysis enables the ease of separation of products from the catalyst since the products may be in a different phase.

An electrocatalyst functions by facilitating electron transfer between an electrode and a substrate, thereby reducing the high electrochemical driving force required for the reaction by providing a lower energy pathway. A good electrocatalyst needs to fulfil certain requirements: it must offer a good catalytic rate constant (k_{cat}) for the reaction it was designed to accelerate, be stable to redox processes, be cheap, efficient, durable and selective in its catalysis, and be easily regenerated. For both CO_2 reduction and water splitting, the electrocatalyst should be reduced to form an intermediate that can transfer electrons to CO_2 to activate it, or to allow for the electrochemical destabilisation H_2O to occur. A number of electrochemical techniques are available to assist in the search for a good electrocatalyst. The most important tools are cyclic voltammetry (CV), linear squarewave voltammetry (LSV) differential pulse voltammetry (DPV) and controlled potential electrolysis (CPE). These electrochemical experiments can yield information for Tafel plots, which relate the overpotential of a reaction to its rate limiting step.[15] A particularly important parameter derived from such plots is the Tafel slope, which yields information about the exchange current density of a reaction and the rate of electron transfer (*i.e.*, the smaller the gradient, the better the electron transfer). Spectroelectrochemistry (SEC) can also be used to provide spectroscopic information about the behaviour of an electrocatalyst *in situ*, which adds another important dimension to the characterisation of an electrochemical reaction and the elucidation of the mechanism of catalysis.[18,42–47] Finally, combining CPE with gas- and solution-phase techniques can assist in identifying and quantifying the catalytic products.

An attractive opportunity for heterogeneous electrocatalysis is metal–organic frameworks (MOFs), which hold promise as a class of highly ordered multifunctional materials that can be readily formed and tuned. Defined by IUPAC as "coordination polymers with an open framework that contain potential voids",[48] frameworks were first reported in 1989[49] and consist of metal ions that are linked together by organic ligands to form scaffolds.[50] A key advantage to MOFs is that they possess high dimensionality, can be robust and are insoluble. It is also possible to tune the components of the MOF in a similar fashion to tuning a discrete homogeneous catalyst.[51] With the large availability of ligands and metal salts, there are a plethora of different MOF topologies that may be synthesised and explored, enabling a move away from precious metals and expensive precursors commonly associated with catalytic processes.[52] Robson *et al.* predicted that the components of frameworks could be rationally chosen to yield a material with desirable functionality – a process known as crystal engineering.[53]

The potential use of MOFs as electrocatalysts is receiving increasing attention as these materials circumvent a number of the limitations of homogeneous catalysts. Through the immobilisation of catalytic sites in MOFs, it may be possible to inhibit deleterious reactions such as dimerisation, since the sites are physically separated in a higher-order structure.

Immobilising catalysts in the solid state with various metal nodes can also impact the electrochemical driving force necessary for electron transfer between the electrode and the catalyst, as well as improving the lifetime of the catalytic site and its selectivity. Additionally, if the MOF has a high internal surface area, a high concentration of catalytic sites should be accessible. It is usually expected that the use of a MOF as an electrocatalyst would require an active surface area, a known propagation of charge, an optimised pore size distribution and good crystallinity.[54] One crucial factor that affects the electrocatalytic performance of a MOF is how well the catalyst is anchored to a conductive surface, since this may allow for charge hopping rather than diffusion to activate any catalytic sites in the MOF.[55]

Methods for the attachment of MOFs to an electrode surface are required to quantify catalyst loading and have been derived from the surface anchoring of discrete complexes. Current approaches to surface attachment involve modifying the conductive surface in order to directly graft functionalised metal complexes. Grafting methods of metal complexes for heterogeneous catalysis have previously been explored,[56–63] and the conductive surfaces used have included carbon nanotubes,[58] graphene,[64] glassy carbon,[65] conductive tin oxides,[66] silver,[67] copper[68] and gold[69] among others. While these surface attachment methods have enabled quantification of catalyst loading, they result in low surface coverage. MOFs as heterogeneous catalysts offer significant potential advantages in terms of the higher number of catalytic sites that may be activated *via* charge hopping mechanisms. As a result, a better understanding of surface fabrication and quantification of heterogeneous catalysis is crucial to enhance their properties and advance the field.

1.1 Scope

With the advent of crystal engineering and a relatively large body of existing literature on photocatalytic MOFs,[70–73] the use of MOFs as electrocatalysts is now gaining pace. Various methods exist for the attachment of MOFs to conductive surfaces – an important consideration to quantify their electrocatalytic activity. This highlight article focuses on the key challenges that have emerged for electrocatalytic MOFs, including aspects of structure that are key to their function, and performance characteristics such as stability and selectivity, in addition to methods for interfacing MOFs with surfaces. Three electrocatalytic conversions processes are discussed, including CO_2 reduction, the hydrogen evolution reaction (HER) and the oxygen evolution reaction (OER), as well as a selection of other relevant catalytic processes. The highlight is restricted to electrocatalysis *intrinsic* to MOFs (that is, where the MOF retains its structural integrity and catalytic properties after CPE), and quantification of the catalysis will be discussed on the basis of Faradaic efficiencies, turnover frequencies (TOFs), turnover numbers (TONs) and Tafel analysis where reported. Readers are additionally directed to a recent comprehensive review on MOF and MOF-derived nanomaterials for electrocatalysis[74] and the use of MOFs as catalyst precursors for catalytic oxides[71,75] (note that these reviews did not address the issue of surface attachment as discussed here).

2. CO_2 reduction

The electrocatalysis of CO_2 reduction requires the presence of coordinatively unsaturated metal sites, or at least metal sites with labile ligands. In the case of homogeneous catalysts, many transition metal systems that interact with CO_2 have been reported, of which the strength and the reversibility of the association with CO_2 is a critical factor.[76] In many examples, the metal–CO_2 bond is strong, which may deactivate the catalytic ability of the transition metal.

From a thermodynamic viewpoint, CO_2 has the capacity to accept an electron to form a $CO_2^{\bullet-}$ radical anion which has provided the impetus for the study of CO_2 electrocatalysis.[15] The $CO_2^{\bullet-}$ radical is a highly energetic species that is observed when CO_2 is reduced at a potential of $E_{pc} = -1.90$ V *vs.* NHE.[20] The Tafel slope for the formation of the radical has previously been reported as 118 mV dec^{-1};[77] therefore, a lower Tafel slope may imply a faster initial electron transfer before a later non-electron transfer rate-determining step.[78] The direct reduction of CO_2 is not favoured thermodynamically due to the large overpotentials associated with the electron transfer. The proton-coupled reduction of CO_2 provides a feasible alternative to direct reduction and can lead to a number of useful products (Table 1).[20,79,80] These products are more thermodynamically favourable than $CO_2^{\bullet-}$; however, the activation energy for their formation is still significant and kinetic penalties are introduced. Since a proton source is required to facilitate CO_2 reduction, it is important that the electrocatalyst does not simply promote reduction of the proton source to H_2 gas (a thermodynamically favoured

Table 1 Reduction reactions of CO_2 and their thermodynamic potentials at neutral pH[79]

Reaction	E^0 (V *vs.* SHE)
CO_2 (g) + $4H^+$ + $4e^-$ → C (s) + $2H_2O$ (l)	+0.210
CO_2 (g) + $2H_2O$ (l) + $4e^-$ → C (s) + $4OH^-$	−0.627
CO_2 (g) + $2H^+$ + $2e^-$ → HCOOH (l)	−0.250
CO_2 (g) + $2H_2O$ (l) + $2e^-$ → $HCOO^-$ (aq) + OH^-	−1.078
CO_2 (g) + $2H^+$ + $2e^-$ → CO (g) + H_2O (l)	−0.106
CO_2 (g) + $2H_2O$ (l) + $2e^-$ → CO^- (g) + $2OH^-$	−0.934
CO_2 (g) + $4H^+$ + $4e^-$ → CH_2O (l) + $4OH^-$	−0.898
CO_2 (g) + $6H^+$ + $6e^-$ → CH_3OH (l) + H_2O^-	+0.016
CO_2 (g) + $5H_2O$ (l) + $6e^-$ → CH_3OH (l) + $6OH^-$	−0.812
CO_2 (g) + $8H^+$ + $8e^-$ → CH_4 (g) + H_2O (l)	+0.169
CO_2 (g) + $6H_2O$ (l) + $8e^-$ → CH_4 (g) + $8OH^-$	−0.659
$2CO_2$ (g) + $2H^+$ + $2e^-$ → $H_2C_2O_4$ (aq)	−0.500
$2CO_2$ + $2e^-$ → $2CO_2^{\bullet-}$ → $C_2O_4^{2-}$ (aq)	−0.590
$2CO_2$ (g) + $12H^+$ + $12e^-$ → CH_2CH_2 (g) + $4H_2O$ (l)	+0.064
$2CO_2$ (g) + $8H_2O$ (l) + $12e^-$ → CH_2CH_2 (g) + $12OH^-$ (l)	−0.764
$2CO_2$ (g) + $12H^+$ + $12e^-$ → CH_3CH_2OH (l) + $3H_2O$ (l)	+0.084
$2CO_2$ (g) + $9H_2O$ (l) + $12e^-$ → CH_3CH_2OH (l) + $12OH^-$	−0.240
$2H^+$ + $2e^-$ → H_2 (g)	+0.000

transformation), but instead has a kinetic preference for CO_2 reduction. The Tafel slope provides useful insight here, since a higher slope may indicate competing reactions with the hydrogen evolution reaction (HER) (*vide infra*).[81,82]

An important factor in catalyst design for the conversion of CO_2 is addressing the kinetic factors associated with its transformation. Despite the thermodynamic incentive to form methane (ΔG° = −130.8 kJ mol^{-1}) or methanol (ΔG° = −17.3 kJ mol^{-1}) in a single step, the relatively simpler two proton, two electron reduction process to fuel precursors has been the subject of much analysis.[20] The reduction of CO_2 to CO is particularly attractive as CO can be converted into liquid fuels *via* Fischer–Tropsch processes[83] and is a feedstock for a number of aldehydes;[84] it is particularly useful on a large scale in metallurgical processes, such as the Mond process for refining Ni.[85] Additionally, the generation of formic acid from CO_2 is an important industrial process because it is useful as a preservative and antibacterial agent, and in the textile industry.[86] The slight thermodynamic penalty for forming CO (ΔG° = +19.9 kJ mol^{-1}) and formic acid (ΔG° = +38.4 kJ mol^{-1}) from CO_2 means that an electrocatalyst is required to assist the transformation.[20]

A number of the early examples of MOFs examined for the reduction of CO_2 contained Cu secondary building units (SBUs). Interest in these Cu frameworks was based on precedence for the reduction of CO_2 at low overpotentials on Cu electrodes, where deposited Cu_2O layers were found to be electrocatalytically active.[87–93] The first reported framework for electrochemical CO_2 reduction was a copper rubeanate MOF reported in 2012 by Yamada *et al.*[94] The as-synthesised MOF particles were mechanically immobilised onto carbon paper to act as the working electrode. Upon CPE at E_{pc} = −1.2 V *vs.* SHE, formic acid was found to be the primary product and was produced in 30% Faradaic efficiency after reaction in aqueous media. The reported overpotentials were lowered by 0.2 V compared to CO_2 reduction on a bare Cu electrode. Characterisation of the framework was achieved using PXRD, elemental analysis and IR, however the definitive structure of the material was not reported. This work serves to highlight a number of challenges in the quantification of electrocatalytic processes involving MOFs including the difficulty in elucidating a reaction mechanism (which often requires a Tafel analysis), their instability under the conditions (structural data such as PXRD is rarely reported post-reaction), and the need for secure attachment of the MOF to the electrode in order to quantify the electroactive surface area.

Work from Kulandainathan *et al.* demonstrated that Cu_3(**btc**)$_2$ could be coated onto glassy carbon using Nafion, a conductive, gas permeable and chemically inert matrix used to adhere the MOF to the surface. CPE was performed on a solution at E_{pa} = −2.5 V *vs.* Ag/Ag$^+$, with the primary product of catalysis found to be oxalic acid, thus providing the first example of a multifunctional MOF that could be used for both the capture and electrochemical conversion of CO_2.[95] The detection of oxalic acid *via* IR spectroscopy occurred at overpotentials that had been lowered by up to 0.65 V, however quantification of the product was not performed. It was suggested that a Cu(I) species was the catalytic agent, however the structural stability of the framework to the catalytic conditions was not thoroughly analysed, nor was Tafel analysis conducted to verify the rate limiting step of the reduction. $^{13}CO_2$-labelled experiments would be useful in the future to verify the source of the product (*i.e.*, oxalic acid generation from CO_2 itself rather than reduction of the solvent, DMF). It is also interesting to note that although Nafion assists the adhesion of the MOF onto the glassy carbon surface, it may also interfere with the properties of the framework, resulting in an inhomogeneous coverage of MOF on the surface and affecting the diffusion of electrons, leading to increased capacitance.[66]

Strategies to address the stability of Cu based MOFs for electrocatalysis have been reported in the work of Albo *et al.*, who investigated both Cu_3(**btc**)$_2$ and [Cu_3(μ-$C_2H_2N_2S_2$)]$_n$ MOFs, as well as metal–organic aerogels for the electrocatalytic reduction of CO_2 to alcohols.[96] The MOFs were deposited onto a gas diffusion electrode (GDE), which is a porous composite electrode constructed from Nafion bonded catalyst particles and a carbon support (carbon paper). The benefit of a GDE is that it can be operated at higher current densities (200–600 mA cm^{-2}) and can form a characteristic gas-solid-liquid three-phase interface, which allows a homogeneous distribution over the catalyst surface and overcomes the limitations of mass transport.[97] However, the presence of Nafion as a binder may also impact the conductive properties of a framework which are important for charge transport within the highly porous electrocatalytic system. The electrodes were characterised using SEM, ATR-IR and PXRD, where homogeneous coverage of MOF was found on the electrode surface. Bulk electrolysis revealed that Cu_3(**btc**)$_2$ and [Cu_3(μ-$C_2H_2N_2S_2$)] could convert CO_2 to methanol and ethanol in Faradaic efficiencies of 15.9% and 1.2%, respectively, with a current density of 10 mA cm^{-2} after optimisation of the electrolyte and gas flow rates. Despite the low conversion of CO_2, catalysis was attributed to unhindered and highly active defect Cu sites in [Cu_3(μ-$C_2H_2N_2S_2$)]. On this basis, it was suggested that focus should be shifted towards MOFs containing bare metal sites for electrocatalysis. Characterisation of the MOF stabilities revealed that Cu_3(**btc**)$_2$ and [Cu_3(μ-$C_2H_2N_2S_2$)] exhibit catalytic behaviour for up to 17 and 12 h, respectively, with gradual deactivation a result of their propensity to undergo hydrolysis in aqueous media.[98] There was also evidence for the formation of malachite (CH_2CuO_2) and leaching of Cu from the carbon support, which are themselves electrocatalytically active, and may have contributed to the observed activity.[99]

A challenge arising from the use of Cu as the active metal for CO_2 electroreduction is that various mixtures of hydrocarbon products are generated, and it is not trivial to improve the selectivity of any specific one.[100–102] The field has therefore expanded to consider other metals that may increase selectivity for certain products of CO_2 reduction, with a particular focus on MOFs incorporating electrocatalytically-active

metals into the SBUs and bare metal sites into the struts. Particular efforts have focused on the incorporation of porphyrins into MOFs, because discrete metal Co and Fe porphyrins have previously been examined as homogeneous electrocatalysts for CO_2 reduction.[103–108] The electrocatalytic conversion of CO_2 to CO was reported in a COF containing 4,4′,4″,4‴-(porphyrin-5,10,15,20-tetrayl)tetrabenzoate)Co(II) (**tcpp-Co**) by Yaghi and co-workers.[109] For electrochemical experiments, the COF was mechanically deposited onto porous, conductive carbon fabric, and an electrochemically active surface concentration of the COF was measured by integrating the reduction wave. CO was formed in Faradaic efficiencies of 90%, with no degradation of the COF observed over the first 24 h of the reaction. This material displayed a high activity for the reduction of CO_2 to CO, achieving TONs as high as 290 000 and an initial TOF of 2.6 s^{-1}. The immobilisation of the porphyrin into the solid state resulted in an improvement in the activity of the catalytic site by a factor of 60. The direct growth of the MOF onto the conductive surface resulted in a lower Faradaic efficiency (86%), but an improvement in the TOF (665 $hour^{-1}$), suggesting that direct methods of surface attachment are necessary to improve electrocatalysis. Tafel analysis on the COF suggested that further mechanistic studies are required, because a higher Tafel slope for the COF (550 mV dec^{-1}) than **tcpp-Co** (270 mV dec^{-1}) itself may indicate that the mechanism of CO_2 reduction is occurring in a different way in the heterogeneous MOF system.

Taking inspiration from the aforementioned COF, the same group incorporated **tcpp-Co** porphyrin into a MOF, where the porphyrin was linked through aluminium oxide rods to generate a 3D framework (Fig. 1A).[110] The MOF was deposited onto ITO through the atomic layer deposition (ALD) of an aluminium oxide layer prior to direct MOF growth.[67] The benefit of ALD lies in the ability to control the defects and thickness of the film,[111] improve deposition times, lower deposition temperatures and increase scalability/repeatability.[112] The direct growth of the MOF onto the surface also removed the need for binders. The electroactive surface of the MOF was quantified using ICP-AES, where an upper concentration limit of Co of 1.1×10^{-7} mol cm^{-2} was obtained. The Co MOF exhibited improved electrocatalytic activity in the presence of CO_2, with an increase in current density from 3.5 to 5.9 mA cm^{-2} at $E_{1/2}$ = −0.5 V *vs.* RHE (Fig. 1C). During CPE, the MOF films demonstrated a high selectivity for the conversion of CO_2 to CO, with TONs of 1400 per catalytic site and a selectivity for CO production in aqueous media with 76% Faradaic efficiency at E_{pc} = −0.7 V *vs.* RHE (Fig. 1D). Spectroelectrochemical experiments suggested that the Co(II/I) redox

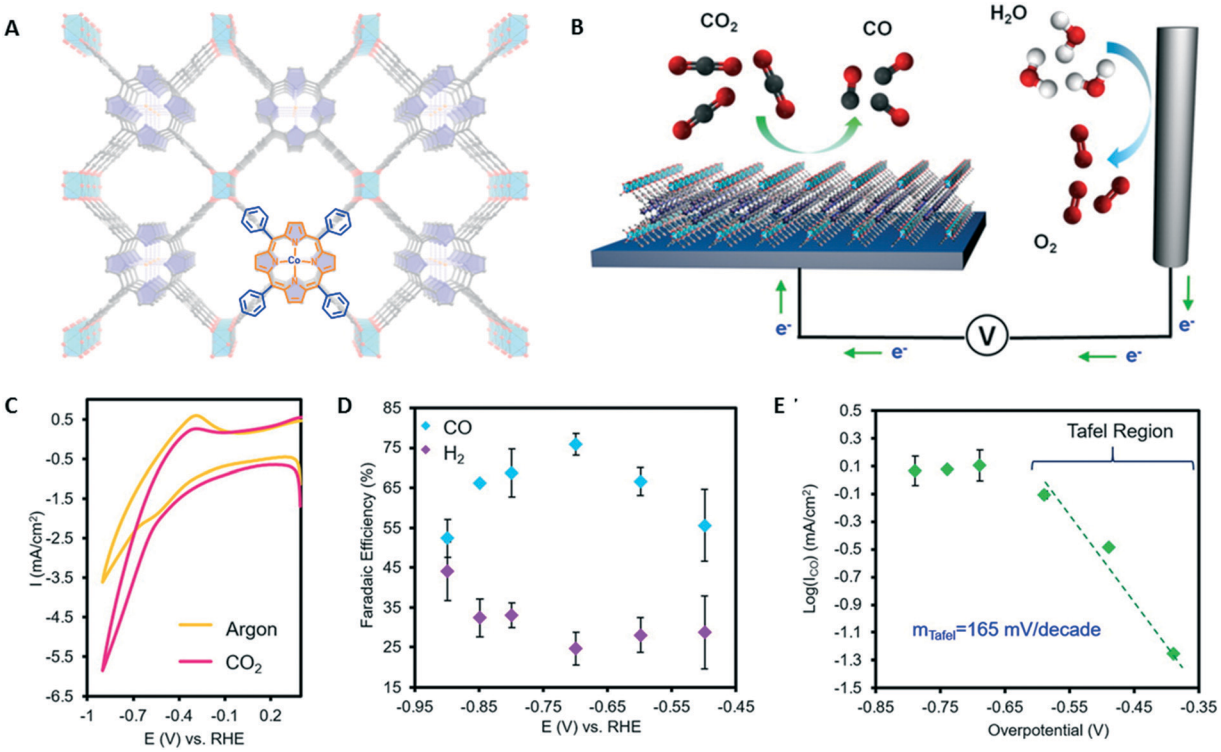

Fig. 1 A: The organic building units in the form of cobalt-metalated **tcpp** are assembled into a 3D MOF, $Al_2(OH)_2$ (**tcpp-Co**). Co: orange spheres; O, red spheres; C, black spheres; N, blue spheres; Al, light-blue octahedra; and pyrrole ring, blue. Each porphyrin is bound to the aluminium organic backbone. B: A schematic of the MOF integrated with a conductive substrate to achieve a functional CO_2 electrochemical reduction system. C: CV of the MOF catalyst exhibiting a current increase in a CO_2 environment relative to an argon-saturated environment. D: The selectivity of CO_2 over H_2 at different potentials, reaching Faradaic efficiencies of up to 76% for CO. E: The Tafel plot for the MOF, with a Tafel slope implying that the one-electron reduction from CO_2 to $CO_2^{\bullet-}$ is the rate limiting step. Adapted with permission from 110.

couple was responsible for the conversion. Tafel plots were examined to gain insight into the mechanism of CO_2 reduction (Fig. 1E), with Tafel slopes ranging from 100–300 mV dec^{-1}, implying that the mechanism involved more steps than those involving the active Co site and the generation of the $CO_2^{\bullet-}$ radical as the rate limiting step. The stability of the MOF was initially evaluated through chronoamperometric measurements and Faradaic efficiency measurements. Physical characterisation of the MOF after CPE (using PXRD, SEM and surface enhanced Raman spectroscopy (SERS)) suggested that the MOF largely retained its crystallinity and morphology after 7 h of CPE.

Fe-porphyrins were chosen for incorporation into MOFs by Hupp and co-workers who electrophoretically deposited (EPD) Fe_MOF-525 onto the conductive substrate FTO.[113] The benefit of EPD is that a powdered form of the MOF can be attached to a highly charged electrode surface by virtue of defects in both the MOF and the surface without the need for a binder. The initial electrochemically accessible surface area was characterised through chronoamperometry, where the current decay over time was recorded and compared to the charge passed. An active surface area of Fe porphyrin of 6.2×10^{-8} mol cm^{-2} was calculated (which is up to 77% of the surface area of the MOF itself). CPE at E_{pc} = −1.3 V *vs.* NHE resulted in the generation of CO and H_2 in a combined Faradaic efficiency of up to 100% (CO = 54%, H_2 = 45%, TON = 272 in the absence of 2,2,2-trifluoroethanol (TFE) and CO = 60%, H_2 = 41% in the presence of TFE). It was suggested that the Fe(I/0) redox couple at $E_{1/2}$ = −1.4 V *vs.* NHE was responsible for the transformation of CO_2 on the basis of evidence from mechanistic studies in the homogeneous systems; namely, a Fe–CO_2 adduct forms that allows for cleavage of a C–O bond and the release of CO.[114,115] The MOF was found to degrade over 5 h, allowing for the release of the homogeneous catalyst into solution, however detailed studies on the degradation of the MOF were not pursued.

In addition to porphyrin-based ligands, the [M(**bpy**)(CO)$_3$X] (M = Mn, Re, **bpy** = 2,2′-bipyridine, X = halogen) complexes are well-known to be good homogeneous electrocatalysts for the proton-dependent reduction of CO_2 into CO with high TOF/TONs and good Faradaic efficiencies.[18,65,116–120] Recently, the incorporation of [Re(**bpy**)(CO)$_3$Cl] into a Zn-paddlewheel based MOF for electrochemical CO_2 reduction was reported by Sun and co-workers (Fig. 2A).[121] Deposition of the MOF onto FTO was achieved *via* liquid-phase epitaxy (LPE), which is a very well established method for the deposition of MOFs onto thin films.[122] LPE has the added benefit of enabling the fabrication of highly oriented and homogeneous MOF thin films with controllable thicknesses.[123] The surfaces were characterised by XRD, suggesting that growth of the MOF was directed along the [001] surface, however, single crystal data was not obtained and the structure was therefore proposed on the basis of Le Bail refinements. Further characterisation through IR and XPS confirmed the incorporation of the [Re(**bpy**)(CO)$_3$Cl] complex into the MOF. CV of the MOF revealed two processes at $E_{1/2}$ = −0.7 and −0.9 V *vs.* NHE, corresponding to the reduction of Re(I/0) and its subsequent loss of chloride, with a noticeable enhancement in current density in the presence of CO_2 (Fig. 2B). CPE was performed on the MOF at E_{pc} = −0.9 V *vs.* NHE for 2 h, with current densities up to 2.5 mA cm^{-2} which were sustained for 30 min. CO production was reported in Faradaic efficiencies up to 93%, an initial TOF of 690 h^{-1} after 30 min and a TON of 580 after 2 h, although these values are based upon an estimation of catalytic sites on an FTO surface (7×10^{-8} mol cm^{-2} assuming a full packing of Re centres on a uniform surface of the electrode) (Fig. 2C). A redox hopping mechanism was proposed for charge propagation in the framework. The proposal of mechanism for CO_2 reduction was based on the behaviour of the homogeneous catalyst, but was not supported by Tafel analysis. The long term stability of the MOF was not addressed.

Han and co-workers reported the first work on the electrochemical reduction of CO_2 using MOFs as a cathode material and ionic liquids (ILs) as the electrolyte to generate the multi-electron reduction product methane (Table 1).[124] The

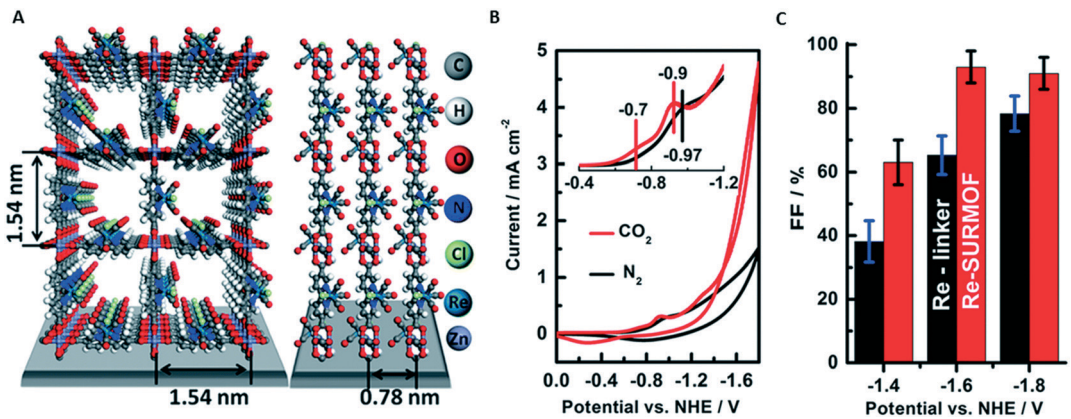

Fig. 2 A: The proposed ideal atomic structure of Re-SURMOF B: CV of Re-SURMOF in saturated electrolyte at a scan rate of 100 mV s^{-1}; C: Faradaic efficiency of Re-SURMOF and Re-linker (0.5 mM) catalysed CO_2 reduction as a function of applied potential. The electrolyte was saturated with CO_2 or N_2. Adapted with permission from 121.

use of ILs hinges on their wide solvent window which allows access more cathodic reduction potentials in MOFs without the IL itself being reduced. Different mass fractions of Zn(**btc**) (based on the Zn node) were deposited onto carbon paper using EPD, with a mixture of 1-dodecyl-3-methylimidazolium (75 wt%) and glycerol (25 wt%) used as the electrolyte. The surface was characterised using PXRD, SEM and SAXS, with XPS used prior to and following EPD to ensure that the MOF retained its structure. The CO_2 reduction studies took place in 1-butyl-3-methylimidazolium tetrafluoroborate, with an enhanced reduction of CO_2 at $E_{1/2}$ = −2.2 V *vs.* Ag/Ag^+. CPE at E_{pc} = −2.2 V *vs.* Ag/Ag^+ for 2 h yielded CH_4 and CO in the gas phase in Faradaic efficiencies of up to 88 and 8%, respectively, depending on the IL used. A Tafel slope of 146 mV dec^{-1} was obtained, suggesting that the rate limiting step of the reaction was the formation of the $CO_2^{\bullet-}$ radical. Only XPS was used to characterise the surface following CPE. It was suggested that the use of the MOF as the cathode demonstrated comparable activity, but higher selectivity for methane production than a traditional metal electrode.

3. Water splitting

An important electrochemically catalysed reaction is the splitting of water into H_2 and O_2, both of which play key roles in the development of clean energy technologies.[125] The formation of O_2 through the oxygen evolution reaction (OER) at the anode and H_2 through the hydrogen evolution reaction (HER) at the cathode usually occur at very high overpotentials, making it critical to include a catalyst for efficient and economical water splitting.[126] Early homogeneous catalysts were based on Ru,[127,128] Ir[129,130] and Pt,[131] however recent efforts have focused on Earth-abundant elements such as Mn,[132] Ni,[133] Cu[134] and Co[135] for scaling the reaction to an industrial level, where discrete Co complexes have already been found to show particularly good activity for OER.[136] Studies on water oxidation have been conducted on discrete metal oxides and layered double hydroxides.[125]

3.1 OER

Traditionally, OER possesses a higher kinetic barrier and sluggish reaction kinetics compared with HER because it is a four electron process and therefore usually requires high performance catalysts.[137] Tafel analysis is difficult in the context of the OER, since there are postulated to be up to five steps involved in the mechanism under alkali conditions (Table 2).[138]

A challenge for OER is the need for alkaline conditions to promote the reaction; however MOFs are not traditionally known to be stable under these conditions.[140] Interestingly, MOF-derived catalysts resulting from decomposition into discrete oxides/hydroxides have been shown to be capable of promoting OER catalysis, however the scope of this review concerns catalysis *intrinsic* to MOFs.

Some of the first examples of coordination polymers that demonstrated intrinsic catalytic behaviour in OER were $Co(\mathbf{bpamb})_{0.5}(\mathbf{adip})$ and $Co_2(\mathbf{bpamb})_2(\mathbf{5\text{-}H_2bdc})_2(H_2O)_2{\cdot}H_2O$ [**bpamb** = 1,4-bis(3-pyridylaminomethyl)benzene, **adip** = adipic acid, **5-H$_2$bdc** = 5-nitro-isophthalic acid], reported by Gong *et al.*[141] Much of the interest in Co-based MOFs stemmed from the observation that many of the discrete homogeneous catalysts for OER contain Co.[142–146] The coordination polymers were immobilised onto glassy carbon using Nafion. For $Co(\mathbf{bpamb})_{0.5}(\mathbf{adip})$ in an aqueous buffer solution (pH = 6.8, H_3PO_4–KOH, 0.2 M), a *quasi*-reversible redox couple was observed at $E_{1/2}$ = +1.07 V *vs.* SCE, and corresponded to the generation of O_2 from water (overpotential is 0.46 V) with an improved current density compared to the bare glassy carbon electrode. The redox activity the coordination polymer was maintained over multiple potential cycles in the CV. CPE was performed at +1.40 V *vs.* SCE for both coordination polymers, where no significant loss of activity over a period of 2 h was observed, which was corroborated by PXRD analysis. Faradaic efficiencies for the evolution of oxygen were estimated to be ~95% with a TON of 2.44, based on the amount of the complex that was used in the synthesis (assuming all sites are catalytically active). Small Tafel slopes were reported, suggesting that there was improved electron transfer, with work on the mechanism to be published in the future.

Pintado *et al.* examined water oxidation using Prussian blue analogues (PBAs) containing Co and Fe.[137] The PBA electrode was formed by electroplating the FTO conductive substrate with Co to improve the anchoring of the PBA, then electrocrystallising the surface at anodic potentials in the presence of hexacyanoferrate(III) to generate the electrode. Surface characterisation was through SEM, PXRD and EDX, which assisted in imaging the surface, determining its crystallinity and evaluating its average stoichiometry ($K_{2x}Co_{(2-x)}[Fe(CN)_6]$, where $0.85 < x < 0.95$). IR studies showed a single CN stretch, suggesting that only coordinated cyanides were present in the sample. CV measurements

Table 2 The OER and its individual mechanism steps under alkali conditions. M represents the electrochemically active site[139]

Equation	E^0 (V *vs.* SHE)	Individual steps
$2H_2O\ (l) \rightleftharpoons O_2\ (g) + 4H^+ + 4e^-$	−1.23	
		$M + OH^- \rightleftharpoons MOH$
		$MOH + OH^- \rightleftharpoons MO + H_2O + e^-$
		$MO + OH^- \rightleftharpoons MOOH + e^-$
		$MOOH + OH^- \rightleftharpoons MOO^- + H_2O$
		$MOO^- + OH^- \rightleftharpoons M + O_2 + e^-$

revealed a *quasi*-reversible oxidation at $E_{1/2}$ = +1.04 V *vs.* NHE and CPE was performed at E_{pa} = +1.41 V *vs.* NHE at pH 7.0, where a steady current was observed (at 35–40% of the initial catalytic current) after one day. The good stability of the material was confirmed by remeasuring the electrodes in new buffer systems, with a measured TOF of 0.7 s^{-1}. Quantitative O_2 evolution was also claimed based upon fluorescence measurements. Tafel analysis revealed slopes in the range of 85–95 mV dec^{-1} suggesting good electron transfer. It was also claimed that no adventitious cobalt oxides were formed on the basis of characterisation of the electrode surface using EDX, and CV/DPV of the electrolyte after electrolysis (which did not yield any additional redox features). Finally, PXRD of the surface post-catalysis suggested that the systems had mostly retained their structures.

The success observed with Co-based MOFs allowed for the investigation into OER using zeolitic imidazolate frameworks (ZIFs), a subclass of MOF topologically analogous to aluminosilicate zeolite structures which exhibit high thermal and chemical stabilities.[147] Co-ZIF-9 was shown to catalyse the OER across a wide pH range by Wang *et al.*[148] The ZIF was immobilised onto FTO with a mixture of Nafion, which was postulated to affect the mediation of electron and proton transfer (Tafel slope = 150 mV dec^{-1}). O_2 evolution was monitored with a fluorescence based sensor, where 8 μmol of O_2 was detected after a 3 h CPE experiment at +1.60 V *vs.* RHE. A TOF of 1.76 × 10^{-3} s^{-1} was calculated, however, no Faradaic efficiency was reported. Furthermore, the electrolyte was made increasingly basic in subsequent electrolysis runs, which resulted in the lowering of the overpotential. The ZIF did not undergo any obvious deactivation over 25 h; however, only XPS was performed to demonstrate its stability after electrolysis.

Porphyrin-based frameworks were further examined to both introduce stability and active bare metal sites into a MOF. The Pb porphyrin MOF [Pb_2(**H_2tccp**)]·4DMF·H_2O was synthesised by Dai *et al.*, and was described as the first 3D Pb-porphyrin MOF which could be used for both gas capture and electrocatalysis.[149] CV studies on the MOF revealed that OER occurs at E_{pa} = +1.70 V *vs.* RHE, and is primarily localised at the framework surface. The TOF was affected by the pH of the solution, and addition of different concentrations of KOH yielded TOFs as high as 5.1 × 10^{-4} s^{-1}. Tafel analysis suggested that surface adsorption was the rate limiting step (Tafel slope = 106–126 mV dec^{-1}). Limited information was available on the nature of the attachment of the MOF to the surface or characterisation of the structure following electrolysis.

Morris and co-workers demonstrated the incorporation of Ni porphyrin into the Zr-based MOF PCN-224, which was found to electrochemically facilitate water oxidation at near neutral pH (Fig. 3A).[150] The water splitting ability of the discrete porphyrin was improved by its incorporation into a MOF containing highly oxophilic metal ions (*i.e.*, Zr(IV)) to improve upon the chemical and structural integrity of the material. The MOF thin film was prepared on FTO *via* a

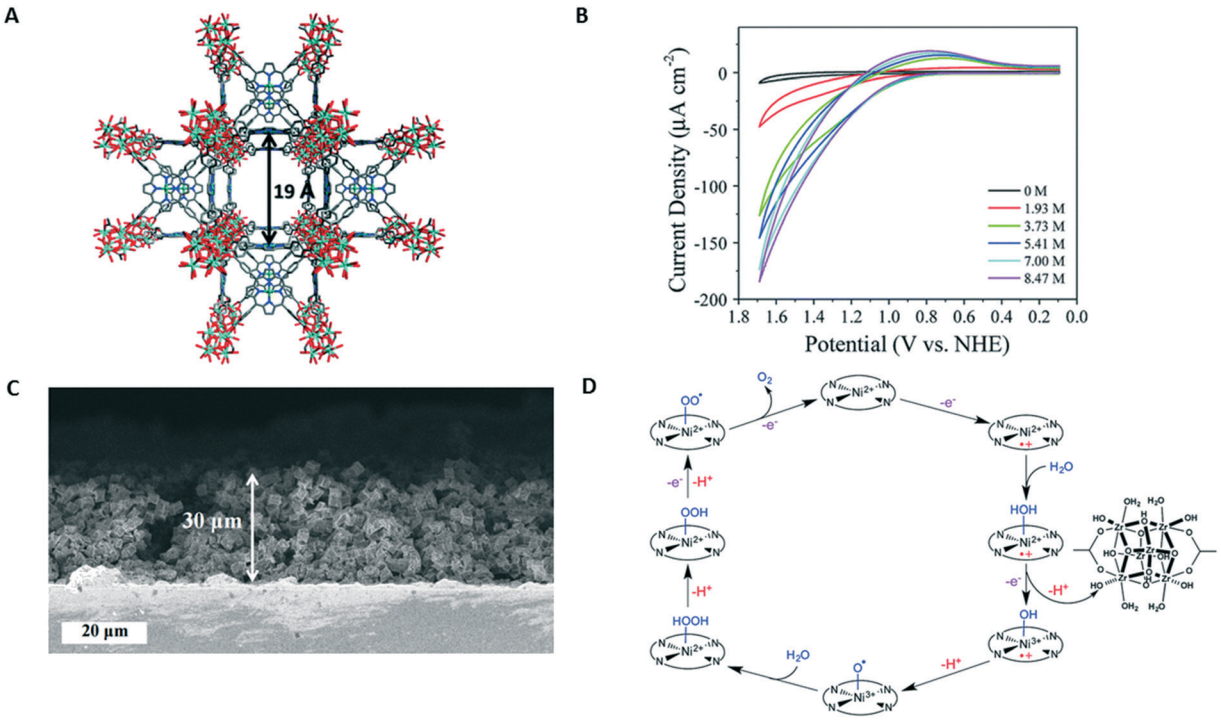

Fig. 3 A: PCN-224 structure with the Ni(II)-to-Ni(II) distance illustrated. Hydrogen atoms have been omitted for clarity. Carbon: grey; oxygen, red; nitrogen, blue; nickel, green; zirconium, light blue B: CV of PCN-224-Ni in 0.1 M $TBAPF_6/CH_3CN$ (black) with increasing H_2O concentrations C: SEM image of solvothermally prepared PCN-224-Ni on FTO showing a film thickness of *ca.* 30 μm D: proposed mechanism for the electrochemical water oxidation reaction catalysed by PCN-224-Ni. Some carboxylate groups have been omitted from the Zr node for clarity. Adapted with permission from 150.

solvothermal reaction of $ZrCl_4$ and Ni(**tcpp**) in the presence of formic acid as a modulator, and the film was characterised using PXRD and SEM (Fig. 3C). For the MOF containing Ni(**tcpp**), the CV revealed an increase in the current density at E_{pa} = +1.0 V *vs.* NHE, which was larger than that for both the blank FTO substrate and the MOF containing a free base porphyrin, suggesting that the oxidation of the Ni(**tcpp**) species was responsible for water splitting (Fig. 3B). The Tafel plot, with a slope of 150 mV dec^{-1} suggested a mechanism in which electrochemical oxidation induces a chemical transformation of oxygen according to Fig. 3C. CPE in 0.1 M $NaClO_4$ at E_{pa} = +1.5 V *vs.* NHE for 60 min revealed a steady current density. To calculate the TOF, the MOF was digested and ICP was used to provide an overestimate of the activity (2×10^{-4} s^{-1}). The Faradaic efficiency was found to be up to 35%. A key result of this work was the proposal and verification of mechanistic steps of the OER using Tafel analysis, taking inspiration from work on the discrete Ni(**tcpp**) (Fig. 3D).[133] This report also provided a detailed characterisation of the MOF thin films following electrolysis using XPS, SEM, ICP and PXRD to demonstrate that there had been significant structural changes.

Post-synthetic exchange (PSE) has also been considered as a viable pathway for introducing electroactivity into a MOF. Lu *et al.* examined ion exchange of the chlorido ligands in the MOF $Co_2(\mu\text{-}Cl)_2$(**btta**) [MAF-X27-Cl, **H$_2$btta** = 1*H*,5*H*-benzo(1,2-*d*:4,5-*d*′)bistriazole] to generate $Co_2(\mu\text{-}OH)_2$(**btta**) [MAF-X27-OH], which dramatically improved the electrocatalytic activity of the MOF. They were also able to demonstrate that the improved activity was linked to the incorporation of the hydroxido ligand which is necessary for catalytic behaviour.[55] Importantly, these frameworks were found to retain their stability in strongly acidic or alkali media for at least one week. The frameworks were mechanically immobilised onto a glassy carbon electrode with a Nafion binder; however, to more accurately evaluate the OER, MAF-X27-Cl was directly grown onto Cu foil and subjected to ion exchange. In the LSV of the framework, the chlorido was replaced by hydroxide anions, as confirmed by a colour change in the MOF and XPS analysis. The surfaces of both MOFs were characterised using Raman, SEM, TEM, PXRD and TGA, where it was found that the morphologies of the frameworks were analogous. When both structures were tested electrochemically, the MAF-X27-Cl framework demonstrated very poor OER behaviour, with a current density of 0.028 mA cm^{-2} at an overpotential of 570 mV, while MAF-X27-OH achieved a current density of 2.0 mA cm^{-2} at an overpotential of 489 mV. To examine the mechanism of OER, IR isotope tracing experiments were performed which demonstrated the direct participation of the hydroxido in the MOF for OER. TOFs of 0.25 s^{-1} at overpotentials of 400 mV were reported with Faradaic efficiencies of 100%. Durability of the frameworks were tested through chronopoteniometry, CV, LSV, PXRD and SEM, where negligible changes were observed following electrolysis.

Wang *et al.* examined Ni(**btc**), Fe(**btc**) and Fe/Ni(**btc**) (with different ratios of Fe : Ni) as possible electrocatalysts for OER.[151] It was found that the heterometallic Fe/Ni(**btc**) MOF possessed an adventitious combination of the lower onset potentials of OER and improved stability of Ni(**btc**) with the larger current densities associated with Fe(**btc**).[152] In particular, the Ni/Fe(**btc**) MOF (Ni : Fe = 12 : 1) demonstrated the most optimal electrocatalytic performance (of those mixtures examined) in alkaline solution with low overpotentials of 270 mV at 10 mA cm^{-2}, and a small Tafel slope of 47 mV dec^{-1}, suggesting good kinetics of electron transfer. In order to avoid the use of binders to immobilise the MOF, EPD was employed to attach the material to Ni foam. PXRD and SEM analysis were used to examine the coverage of the Ni foam electrodes and the crystallinity of the MOF, while EDX and ICP-AES were used to quantify the amount of MOF attached to the surface and demonstrate that both Ni and Fe sites were homogeneously distributed across the surface. CPE was performed at E_{pa} = +1.53 V *vs.* RHE, where O_2 was observed by gas chromatography, with a Faradaic efficiency of 95% and a TOF of 468 h^{-1} (which was based on the amount of Ni present in the sample, as calculated from ICP analysis). Characterisation of the films was conducted after 15 h of CPE using SEM, XPS, IR and PXRD, with no apparent degradation observed.

3.2 HER

HER is an important reaction for the generation of energy,[153–155] with a two-step mechanism invoked for the reaction. The first step involves the adsorption of one H onto the catalyst surface (Volmer step), followed by either the reaction of the adsorbed H with an H^+ (Heyrovsky step) or another adsorbed H (Tafel step) (Table 3). Tafel plots have been widely employed to gain insight into the reaction mechanism. Like the OER, HER is also affected by pH, such that MOFs that are stable to acidic conditions are desired. The benchmark for all HER catalysts is Pt, where the onset potential for a bare Pt catalyst is −0.24 V *vs.* SCE.[156] It is hoped that using MOFs could reduce current overpotentials to this level.

Only a couple of reports in the literature have emerged where HER results from the intrinsic catalytic activity of the MOF. In these cases, Co, Cu, Ni and Zn are the metals that are usually chosen as the nodes. The work of Gong *et al.* examined MOFs based upon 4-(5-(pyridin-4-yl)-4*H*-(1,2,4-triazol-3-yl) benzoic acid (**pytriben**) for synthesis of M_2(**pytriben**)$_4$ $\cdot 3H_2O$ [M = Co, Cu, Zn].[157] This work revealed that the Co and Cu analogues displayed electrochemical activity for HER, suggesting that the origin for the catalysis was the metal cluster. Samples were immobilised onto glassy carbon with Nafion as a binder. CVs of the electroactive frameworks were performed, where Co_2(**pytriben**)$_4 \cdot 3H_2O$ exhibited a weak one-electron reduction at $E_{1/2}$ = −0.90 V *vs.* SCE and a catalytic onset for H^+ reduction at E_{pc} = −1.30 V *vs.* SCE (overpotential = −0.66 V); in comparison, Cu_2(**pytriben**)$_4 \cdot 3H_2O$ exhibited a weak one-electron reduction at $E_{1/2}$ = −0.93 V *vs.* SCE with the catalytic onset of H^+ reduction at −1.40 V *vs.* SCE (overpotential = −0.76 V). Water oxidation was also observed at

Table 3 The HER and its individual mechanism steps in acidic conditions[156]

Reaction	Equation	E (V *vs.* SHE)	Tafel slope (mV dec^{-1})
HER	$4H^+ + 4e^- \rightleftharpoons 2H_2$ (g)	0.00	
Volmer step	$H^+ + e^- \rightarrow H_{ad}$		120
Heyrovsky step	$H^+ + H_{ad} \rightarrow H_2$ (g)		40
Tafel step	$2H_{ad} \rightarrow H_2$ (g)		30

+1.05 and +1.37 V *vs.* SCE (overpotential = +0.46 V, +0.78 V) for Co_2(**pytriben**)$_4$·3H_2O and Cu_2(**pytriben**)$_4$·3H_2O, respectively. While Tafel plots were provided to demonstrate lowered overpotentials in the presence of the MOF (compared with the blank glassy carbon and the organic linker), the mechanism of HER was not well explored. CPE was performed at E_{pc} = −1.50 V *vs.* SCE for HER and +1.40 V *vs.* SCE for OER, where the catalyst for H_2 and O_2 were operating at 98% Faradaic efficiency. TONs of 1.92 and 1.29 (for H_2), and 6.73 and 2.25 (for O_2) were recorded for Co_2(**pytriben**)$_4$·3H_2O and Cu_2(**pytriben**)$_4$·3H_2O, respectively. The glassy carbon was characterised by PXRD after HER electrolysis, confirming that the structures of the MOFs had been retained, while the bulk electrolysis solution was examined using UV-vis-NIR, with no evidence for leaching of the metal centres. For OER, there was evidence for catalyst degradation, but this was not quantified. Given the improved electrocatalytic behaviour observed for the Co catalyst, the work was followed-up by further reports of two Co-based MOFs based on 4,5-di(4′-carboxylphenyl)phthalic acid (**cppa**), namely [Co_4(**cppa**)(**bpy**)-(H_2O)·3.5H_2O] and [Co_2(**cppa**)(**azene**)(H_2O)$_3$·DMF] (**azene** = (*E*)-1,2-di(pyridin-4-yl)diazene), where similar catalytic ability from the metal centre was observed.[158]

Success for HER has also been demonstrated in a class of MOFs that incorporate polyoxometallates (POMs), which are well-known to possess good catalytic activity. POMs are soluble anionic metal oxide clusters of transition metals in high oxidation states (such as W(IV), Mo(V/VI) or V(IV,V) among others) that have previously been used as molecular electrocatalysts.[159] Their solubility has enabled their incorporation into a number of MOFs, where the metal nodes acts as the SBUs in the MOF (defined as a POMOF).[160] POMOFs are usually synthesised under acidic conditions, and are therefore functional with minimal degradation in acidic media and are highly redox-active.[161] POMs may also be incorporated into MOFs through their encapsulation or anchoring to the MOF surface. These are referred to as POM-based MOF materials and are not examined in this article.[162]

Dolbecq and co-workers incorporated a Mo-based POM into a series of POMOFs and investigated their electrocatalytic activity towards the HER.[163,164] In their initial studies, three novel POMOFs were generated hydrothermally consisting of [$PMo(IV)_8Mo(VI)_4O_{36}(OH)_4Zn_4$] and **btc** ligands, with channels occupied by tetrabutylammonium counter cations (Fig. 4A).[163] The electrodes were fabricated through the

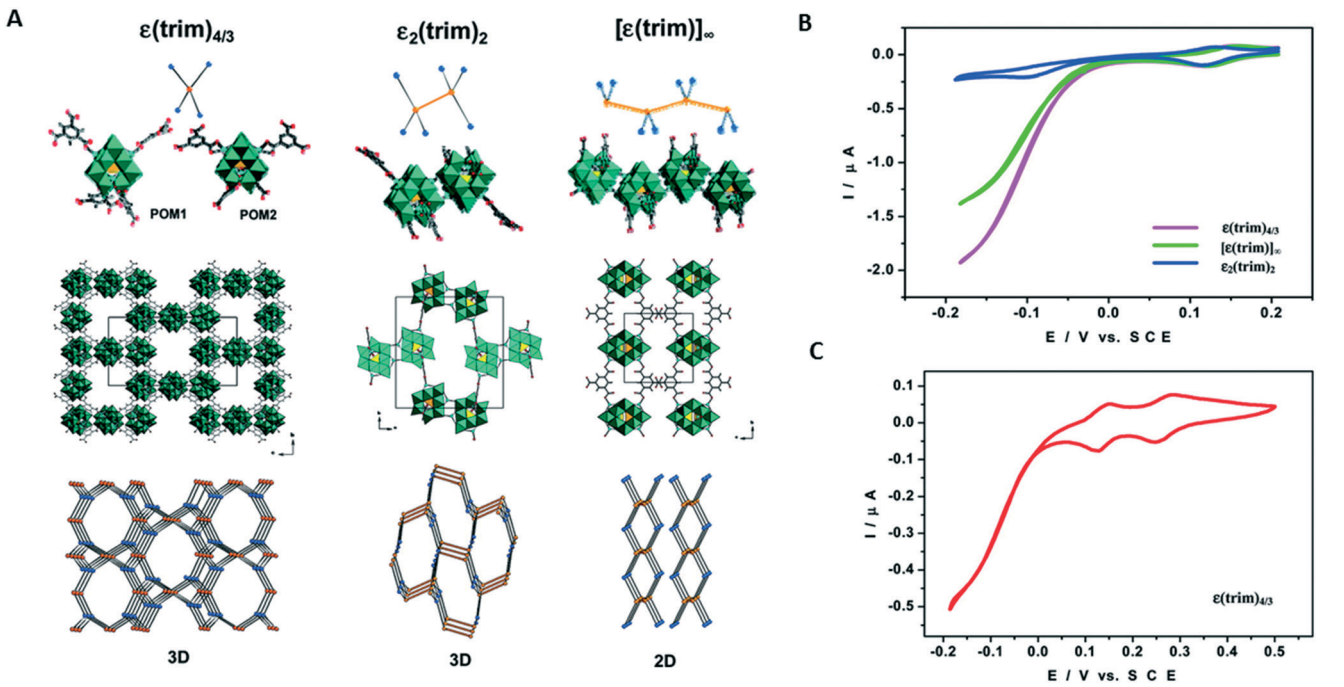

Fig. 4 A: POM building blocks of ε(**trim**)$_{4/3}$, ε_2(**trim**)$_2$, and [ε(**trim**)]$_\infty$, a view of their unit cell, and their schematic representation; black lines indicate connections between POMs and trim linkers, while orange lines symbolize condensation reactions between POMs. B: Comparison of ε(**trim**)$_{4/3}$, ε_2(**trim**)$_2$, and [ε(**trim**)]$_\infty$ at a scan rate of 2 mV s^{-1}, highlighting the catalytic process. The reference electrode was SCE. C: CVs observed for the oxidized form ε(**trim**)$_{4/3}$/CPE as a function of potential scan rate in a (1 M LiCl + HCl (pH 1)) medium at scan rate of 2 mV s^{-1}. Adapted with permission from 163.

preparation of a carbon paste electrode containing the MOFs. CVs of these POMOFs demonstrated two Mo-reduction waves, corresponding to the reversible reduction of Mo(VI/IV).[165] The electrodes could be recycled hundreds of times without significant alteration, while a number of electrodes were left in air for months and tested without any significant diminution of activity. Intercalation of Li^+, Na^+ and K^+ into the POMOF was studied, where it was shown that HER was still observed, with the Li^+ intercalation exhibiting the best activity. HER was detected at an onset potential of E_{pa} = +0.20 V *vs.* SCE, which corresponds to a lowering in the overpotential by 260 mV compared with Pt itself, in Faradaic efficiencies above 95% and a TON as high as 1.2×10^5 over 5 h (TOF = 6.7 s^{-1}, which exceeds the activity of the Pt metal benchmark in HER catalysis). The structural stability of the materials towards the electrochemical process was not discussed in detail, however a mechanism for HER was tentatively proposed. Later studies by this group focused on the effect of different organic linkers in the POMOF for HER, where it was revealed that HER catalysis depended primarily on the presence of the $[PMo(IV)_8Mo(VI)_4O_{36}(OH)_4Zn_4]$ SBU.[164]

Using the $[PMo(IV)_8Mo(VI)_4O_{36}(OH)_4Zn_4]$ POM, Zhou and co-workers reported the synthesis of two novel POMOFs containing benzene tribenzoate (**btb**) and 1,1′-biphenyl]-3,4′,5-tricarboxylate (**bpt**), which were found to exhibit good stability in both acidic and basic media.[166] The POMOFs (50 wt%) were attached to a glassy carbon electrode in a mixture of carbon black (50 wt%). CVs for {$[PMo(IV)_8Mo(VI)_4O_{36}(OH)_4Zn_4]$(**btb**)} exhibited three redox processes at $E_{1/2}$ = −0.091, +0.176 and +0.296 V *vs.* SCE while {$[PMo(IV)_8Mo(VI)_4O_{36}(OH)_4Zn_4]$(**bpt**)} showed three redox processes at $E_{1/2}$ = −0.092, +0.177 and +0.288 V *vs.* SCE. Scan rate dependence studies revealed that the redox processes were surface controlled. Bulk electrolysis on {$[PMo(IV)_8Mo(VI)_4O_{36}(OH)_4Zn_4]$(**btb**)} confirmed its highest activity among all MOF materials reported to date for HER, with an onset potential of E_{pa} = +0.18 V *vs.* SCE (overpotential = 237 mV). The activity of the composite was improved over that of carbon or the POMOF itself, suggesting that the carbon black aids in increasing the current density, while the POMOF lowers the overpotential. The Tafel analysis of both frameworks yielded a slope of 96 mV dec^{-1} for {$[PMo(IV)_8Mo(VI)_4O_{36}(OH)_4Zn_4]$(**btb**)} and 137 mV dec^{-1} for {$[PMo(IV)_8Mo(VI)_4O_{36}(OH)_4Zn_4]$(**bpt**)}, suggesting a good current exchange for HER. The POMOFs were also found to maintain their electrocatalytic activity after 2000 cycles. PXRD patterns were measured for both POMOFs after immersion of the as-synthesised material into an acidic solution for 6 h, where there was limited change, supporting the retention of structure of the MOFs under the electrocatalytic conditions.

From these initial findings on POMOFs, studies have sought to vary the identity of the POM to improve the catalytic behaviour of the framework by addition of electrocatalytically active metals. This includes the work on 1D chains containing unsaturated metal centres based on $Cu_8(Mo_8O_{26})$(**atri**)$_4$ [**atri** = 4*H*-4-amino-1,2,4-triazole] and $Ag_4(Mo_8O_{26})$(**dmatri**) [**dmatri** = 3,5-dimethyl-4-amino-4*H*-1,2,4-triazole). Although these materials are not technically MOFs,[48] the results of this study are pertinent to the discussion.[161] The surfaces were fabricated by dispersing the MOF in Nafion and adhering it to a glassy carbon surface. Both the Cu and Ag based chains exhibited improved H_2 generation, with the Cu chain possessing higher activity than its Ag counterpart. As a specific example, the electrocatalytic behaviour of $Cu_8(Mo_8O_{26})$(**atri**)$_4$ was examined using CV, where the onset potential for HER was −0.67 V *vs.* Ag/AgCl (overpotential = −0.53 V) and was accompanied by an increase in the current density. CPE at −0.8 V *vs.* Ag/AgCl revealed a linear build-up of charge over time, with a Faradaic efficiency of 98% for the production of H_2 and a TON of 2.6×10^3 over 2 h.

4. Other types of catalysis

Catalysis in MOFs is not only limited to the aforementioned classes discussed here, and a number of other industrially relevant processes where electrocatalytically active MOFs may be relevant have been reported. A particular driving force has been the need to improve the viability of alternative fuel supplies, such as water and direct alcohol fuel cells, and to find a way to efficiently remove potentially harmful pollutants from the atmosphere. In many cases, Pt, Pd and Ru catalysts play central roles in current technologies, however these metals are expensive, and are increasingly becoming scare. A serious need therefore exists for alternative materials, such as MOFs, to function in these processes.

The oxygen reduction reaction (ORR) is an important process that has gained particular attention for possible applications in fuel cells. The limitation that exists for a large scale reaction in the current environment is that Pt-based catalysts have been essential in improving upon the slow kinetics associated with the reaction.[167] The expense associated with Pt group metals has seen developments in using metal oxides and carbon-based non-noble and metal free catalysts; however, there is still a significant way to go before these materials will become competitive with the noble-metal candidates in the literature. There has been increased attention on the use of MOFs for electrocatalysis, offering potential as a more economical alternative to improve upon the slow rates of reaction and limited activity of the four electron reduction reaction which is thermodynamically and kinetically challenging.[167] The use of MOFs as a class of low-platinum catalysts for the reaction has already been extensively examined in previous reviews.[54,74,167–169]

MOFs have also been used as candidates for a number of other electrocatalysis reactions (Table 4). In particular, a number of these simpler catalysis reactions and the attachment of the MOFs examined onto surfaces has allowed for studies into the differences between heterogeneous MOF catalysis and homogeneous catalysis, paving the way for improved mechanistic studies for catalytically-active MOFs. Morris and co-workers reported the direct growth of a Co porphyrin Co(**tcpp**) onto FTO substrates for the purpose of

Table 4 Examples of electrocatalysis that has been performed using MOFs and the method of surface attachment employed for its quantification

Type of catalysis	MOF used	Surface attachment method	Ref.
Alcohol oxidation	$(HOC_2H_4)_2$(**dtoa**)Cu	Mechanical immobilisation with Nafion	171, 172
	(**maa**)Cu_3(**btc**)$_2$	Self assembled monolayers on gold	173
	(**ta**)Cu_3(**btc**)$_2$		
	Cu_2(**bpy**)$_2$(**btc**)	Mechanical immobilisation	174
Hydrazine oxidation and nitrobenzene reduction	Co_2(**4-ptz**)$_2$(**bpp**)$(N_3)_2$	Dip coating	175
Nitrite oxidation	MOF-525	Direct crystallisation onto FTO	176
Peroxide oxidation	[Cu(**adp**)(**bib**)$(H_2O)]_n$	Drop casting onto glassy carbon	177
Dopamine oxidation and nitrobenzene reduction	MIL-101	Immobilised in a carbon paste electrode	178
Halide reduction	Co(**tcpp**)	Solvothermal deposition	170
	Fe_2NiO(**piv**)$_6$(**bptz**)$_x$	Mechanical immobilisation	179
	Fe_2NiO(**piv**)$_6$(**bptztz**)$_x$		
	[**TBA**]$_6$[$H_3PMo_{12}O_{40}]_2$[Zn_8(**btb**)$_2$]	Immobilised in a carbon paste electrode	180

H_2**dtoa** = dithiooxamide, **maa** = mercaptoacetic acid, **btc** = 1,3,5-benzenetricaboxylic acid, **ta** = trimesic acid, **bpy** = 2,2′-bipyridine, **4-ptz** 5-(4-pyridyl)tetrazole, **bpp** = 1,3-bi(4-pyridyl)propane, **adp** = adipic acid, **bib** = 1,4-bisimidazolebenzene, H_4**tcpp** = *meso*-tetra(4-carboxyphenylporphyrin **piv** = 2,2-dimethylpropanoic acid **pca** = 4-pyridinecarboxylic acid **pcb** = 2-pyridinecarbaldehyde, **tcpp** = 5,10,15,20-(4-carboxyphenyl)porphyrin, **bptz** = 3,6-(4-pyridyl)-1,2,4,5-tetrazine, **bptztz** = 2,5-di-(4-pyridyl)-thiazolo[5,4-*d*]thiazole, **btb** = 1,3,5-*tris*-(4-carboxyphenyl)-benzene.

reducing CCl_4.[170] An increase in the current density was observed in the framework using CV, while spectroelectrochemical measurements throughout the catalysis indicated that there were limited changes in the framework. Long term CPE measurements were also performed, where no significant short term deterioration of the film was observed (through SEM analysis), and no additional absorption features were apparent in measurements of the electrochemical solution. A slow deterioration of the Co SBU cluster and release of the Co(**tcpp**) was proposed in the longer term. Although the quantification of CCl_4 reduction was not pursued, the immobilisation of the framework onto the FTO surface allowed for conductivity measurements to be performed, which showed that despite the framework being insulating in nature, charge transfer occurred through a hopping mechanism (Fig. 5).

The theoretical mechanism for the electrochemical oxidation of ethanol by $(HOC_2H_4)_2$(**dtoa**)Cu was proposed and experimentally confirmed by Kitagawa and co-workers.[171] Analogues of the MOFs R_2(**dtoa**)(Cu) [R = HOC_3H_6, C_2H_5, C_3H_7, CH_3, H] were also examined and related to the theoretical results. The MOFs were immobilised onto the surface as mixture with Nafion. The proton transfer reaction for the oxidation was first considered using DFT, where it was determined that the proton was transferred from the ethanol to the HOC_2H_4, which was energetically more favourable than an indirect transfer. To confirm this, ethanol sorption isotherms were employed to observe changes in the hysteresis of the ethanol, where a shorter hydroxyl chain on the SBU yielded a smaller hysteresis, suggesting a lower adsorption energy. The increase in the current density and change in peak shape in the CV of the MOF upon the titration of ethanol revealed that electrooxidation of ethanol was occurring. CPE experiments were subsequently performed on the MOFs, where only acetaldehyde was detected in Faradaic efficiencies of 4.6% for $(HOC_3H_6)_2$(**dtoa**)Cu and 6.8% for $(HOC_2H_4)_2$(**dtoa**)Cu, confirming that the mechanism proceeds *via* a direct protonation. Although electroxidation reaction activity was reported for $(C_2H_5)_2$(**dtoa**)Cu, no Faradaic efficiency was determined. Despite the mechanism of reduction being examined in the MOF, and supported by DFT calculations, experimental data on the structural stability of the MOF following catalysis and the mechanism were not reported.

Surface attachment has largely been considered as a viable option for improving the stability of MOFs in aqueous solution. Vulcu *et al.* examined the tethering of Cu_3(**btc**)$_2$ to a gold surface using mercaptoacetic acid and trimesic acid to gold surfaces.[173] When not attached to a surface, Cu_3(**btc**)$_2$ was found to retain its structure with water present up to 0.5 mol of the copper content of the framework.[181] Additional water would result in the decomposition of the MOF, which has negative ramifications for electrocatalysis in aqueous media. The surface was prepared through anodisation of the gold, prior to the generation of a self-assembled monolayer of mercaptoacetic or trimesic acid, and immersion of the gold in a solution of the framework to allow for crystallisation of Cu_3(**btc**)$_2$. Not only did this allow for the selective orientation of the MOF along the [111] axis, but also a

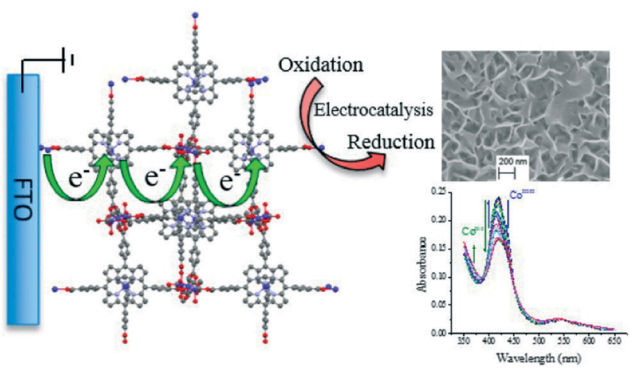

Fig. 5 A schematic attachment of the Co(**tcpp**) MOF onto a FTO and its proposed charge hopping mechanism. Reproduced with permission from 170.

significant enhancement in the current density of the anchored MOF was observed in the presence of methanol, suggesting that surface anchoring improves the electrochemical response of $Cu_3(\mathbf{btc})_2$. These results were compared to the bare gold electrode, the self-assembled monolayer and the deposited MOF on the surface in H_2SO_4, suggesting that the catalytic ability arises from a combination the MOF and the methanol. When the MOF was drop cast onto glassy carbon, no activity was reported for the MOF, suggesting that immobilisation onto a surface is essential for activity to be achieved. The stability of the electrodes was examined through chronoamperometry, suggesting that there was degradation of the surface after approximately 20 min.

5. Conclusions and perspectives

As is evident from the examples described above, there is an excellent opportunity to exploit redox-activity of MOFs for use as electrocatalysts.[34] Significant progress has already been made to identify key structural features of MOFs that make them suitable for catalysis, upon which further improvements will no doubt be forthcoming. One of the greatest challenges that currently exists is the long term stability of the frameworks. If the MOF degrades upon catalysis, the discrete complexes responsible for catalysis may be released into solution as homogeneous catalysts, making the elucidation of mechanism difficult. Currently, a significant amount of literature exists concerning the use of pyrolysis of MOF precursors as a platform for generating catalytically active species, as well as the controlled decomposition of frameworks to catalytic oxides.[75,182–184] As a result, there has been an increase in studies to improve the structural integrity of MOFs. One such pathway has been the design of MOFs with increased stability in aqueous media, particularly at acidic and basic pH levels. There is also scope to explore MOF hybrids to improve the integrity of frameworks while maintaining their tunability. Studies into MOF/polymer (polyMOFs)[185,186] and MOF/carbon composites are currently underway to develop and exploit synergistic properties which may enhance the catalytic performance, as has already been observed.[166]

The selectivity for generating desirable electrocatalytic products is also a key concern. In the context of CO_2 reduction for example, it was observed that metals such as Cu would yield many different hydrocarbon products.[100–102] Likewise, H_2 production often competes with electrocatalysis, since it is generated at lower overpotentials than other carbon based fuels.

A further key issue that underlies electrocatalytic performance is the intrinsic electronic conductivity of the MOF, which facilitates charge propagation.[34] As noted above, some studies have sought to improve conductivity of insulating and semi-conducing MOFs by immobilising them in a conductive matrix such as carbon black or Nafion. An alternative strategy lies in improving the intrinsic conductivity of the MOF, and significant recent strides have been made in this area, though more specifically within the context of electronic devices for applications such as chemisensors.[187–189]

Although significant advances have been made in methods for the attachment of frameworks to surfaces, a number of the challenges remain to be overcome. To date, the majority of methods have involved the addition of a conductive binder, such as Nafion, which has previously been shown to diminish the electrocatalytic performance of a MOF due to the different kinetics of charge transfer. Likewise, during catalysis, if there is no strong anchoring, the MOF may detach from the surface, affecting the calculation of reliable Faradaic efficiencies, TONs and TOFs. Moreover, insight into the mechanism of electrocatalytic processes, which are relatively poorly understood at the present time, is significantly convoluted if detachment or dissolution occurs during the process. Computational modelling studies will offer important insights, as they have for homogeneous systems, with the additional complication of addressing the infinite periodic structure of the MOF. Nevertheless, progress is being made in this area, which will lead to improved understandings of how heterogeneous processes differ from their homogeneous counterparts.

A number of additional areas will help propel the field of electrocatalytic MOFs forward, including the scope to explore the deliberate incorporation of defects into MOFs. Defect sites can assist in improving surface attachment techniques such as EPD, and can themselves act as the active sites for electrocatalysis. Designing oriented films may also improve the selectivity for desired products. Finally, new and interesting high throughput techniques for surface attachment, such printing MOF inks onto electrodes are being explored, and offer alternate avenues to achieve surface adhesion of MOFs.[190]

While a number of challenges remain to be addressed, this perspective article has sought to highlight the significant opportunities that exist for electrocatalytic MOFs, and the key areas which are deserving of future research efforts.

Acknowledgements

This work was supported by the Australian Research Council and the Science and Industry Endowment Fund (SIEF) as part of the 'Solving the Energy Waste Roadblock' venture. We gratefully acknowledge Dr Danielle Kennedy at the Commonwealth Scientific and Industrial Research Organisation (CSIRO) for her support in the provision of an OCE PhD top-up scholarship for MBS. We are also grateful to Dr Charles Machan from The University of Virginia for his helpful comments on an initial version of the section on CO_2 electrocatalysis.

References

1 R. Carapellucci, L. Giordano and M. Vaccarelli, *Energy Procedia*, 2015, **82**, 350–357.

2 R. Wennersten, Q. Sun and H. Li, *J. Cleaner Prod.*, 2015, **103**, 724–736.
3 G. A. Olah, G. K. S. Prakash and A. Goeppert, *J. Am. Chem. Soc.*, 2011, **133**, 12881–12898.
4 D. M. D'Alessandro, B. Smit and J. R. Long, *Angew. Chem., Int. Ed.*, 2010, **49**, 6058–6082.
5 J.-R. Li, Y. Ma, M. C. McCarthy, J. Sculley, J. Yu, H.-K. Jeong, P. B. Balbuena and H.-C. Zhou, *Coord. Chem. Rev.*, 2011, **255**, 1791–1823.
6 E. S. Rubin, J. E. Davison and H. J. Herzog, *Int. J. Greenhouse Gas Control*, 2015, **40**, 378–400.
7 R. Barker, Y. Hua and A. Neville, *Int. Mater. Rev.*, 2016, 1–31, DOI: 10.1080/09506608.2016.1176306.
8 J. Liu, P. K. Thallapally, B. P. McGrail, D. R. Brown and J. Liu, *Chem. Soc. Rev.*, 2012, **41**, 2308–2322.
9 J.-R. Li, R. J. Kuppler and H.-C. Zhou, *Chem. Soc. Rev.*, 2009, **38**, 1477–1504.
10 J. O. M. Bockris, *Int. J. Hydrogen Energy*, 2002, **27**, 731–740.
11 A. Schmid, J. S. Dordick, B. Hauer, A. Kiener, M. Wubbolts and B. Witholt, *Nature*, 2001, **409**, 258–268.
12 A. Fürstner, *Angew. Chem., Int. Ed.*, 2014, **53**, 8587–8598.
13 M. C. Holland and R. Gilmour, *Angew. Chem., Int. Ed.*, 2015, **54**, 3862–3871.
14 S. Kaufhold, L. Petermann, R. Staehle and S. Rau, *Coord. Chem. Rev.*, 2015, **304–305**, 73–87.
15 J. Wang, *Analytical Electrochemistry*, John Wiley & Sons, New Jersey, 2006.
16 I. R. Shaikh, *J. Catal.*, 2014, **2014**, 35.
17 S. C. Roy, O. K. Varghese, M. Paulose and C. A. Grimes, *ACS Nano*, 2010, **4**, 1259–1278.
18 J. Hawecker, J.-M. Lehn and R. Ziessel, *J. Chem. Soc., Chem. Commun.*, 1984, 328–330.
19 J. Albo, M. Alvarez-Guerra, P. Castano and A. Irabien, *Green Chem.*, 2015, **17**, 2304–2324.
20 E. E. Benson, C. P. Kubiak, A. J. Sathrum and J. M. Smieja, *Chem. Soc. Rev.*, 2009, **38**, 89–99.
21 Y. Li and Q. Sun, *Adv. Energy Mater.*, 2016, **6**, 1600463, DOI: 10.1002/aenm.201600463.
22 C. Costentin, M. Robert and J.-M. Saveant, *Chem. Soc. Rev.*, 2013, **42**, 2423–2436.
23 J. R. McKone, S. C. Marinescu, B. S. Brunschwig, J. R. Winkler and H. B. Gray, *Chem. Sci.*, 2014, **5**, 865–878.
24 M. T. M. Koper and E. Bouwman, *Angew. Chem., Int. Ed.*, 2010, **49**, 3723–3725.
25 M. Wang, L. Chen and L. Sun, *Energy Environ. Sci.*, 2012, **5**, 6763–6778.
26 V. S. Thoi, Y. Sun, J. R. Long and C. J. Chang, *Chem. Soc. Rev.*, 2013, **42**, 2388–2400.
27 G. A. N. Felton, C. A. Mebi, B. J. Petro, A. K. Vannucci, D. H. Evans, R. S. Glass and D. L. Lichtenberger, *J. Organomet. Chem.*, 2009, **694**, 2681–2699.
28 T. Reier, H. N. Nong, D. Teschner, R. Schlögl and P. Strasser, *Adv. Energy Mater.*, 2016, 1601275, DOI: 10.1002/aenm.201601275.
29 D. J. Wasylenko, R. D. Palmer and C. P. Berlinguette, *Chem. Commun.*, 2013, **49**, 218–227.
30 J. J. Concepcion, J. W. Jurss, M. K. Brennaman, P. G. Hoertz, A. O. T. Patrocinio, N. Y. Murakami Iha, J. L. Templeton and T. J. Meyer, *Acc. Chem. Res.*, 2009, **42**, 1954–1965.
31 H. Wendt, *Electrochim. Acta*, 1984, **29**, 1513–1525.
32 M. R. Gogate, *Chem. Eng. Commun.*, 2017, **204**, 1–27.
33 G. Pliego, J. A. Zazo, P. Garcia-Muñoz, M. Munoz, J. A. Casas and J. J. Rodriguez, *Crit. Rev. Environ. Control*, 2015, **45**, 2611–2692.
34 D. M. D'Alessandro, *Chem. Commun.*, 2016, **52**, 8957–8971.
35 E. Roduner, *Chem. Soc. Rev.*, 2014, **43**, 8226–8239.
36 Z. Chen, J. J. Concepcion, J. W. Jurss and T. J. Meyer, *J. Am. Chem. Soc.*, 2009, **131**, 15580–15581.
37 C. M. Lieber and N. S. Lewis, *J. Am. Chem. Soc.*, 1984, **106**, 5033–5034.
38 T. Yoshida, K. Tsutsumida, S. Teratani, K. Yasufuku and M. Kaneko, *J. Chem. Soc., Chem. Commun.*, 1993, 631–633, DOI: 10.1039/C39930000631.
39 C. Zhang, J. Tang, C. Peng and M. Jin, *J. Mol. Liq.*, 2016, **221**, 1145–1150.
40 R. T. Vang, E. Laegsgaard and F. Besenbacher, *Phys. Chem. Chem. Phys.*, 2007, **9**, 3460–3469.
41 G. A. Somorjai, *Langmuir*, 1991, **7**, 3176–3182.
42 J. Desilvestro and S. Pons, *J. Electroanal. Chem. Interfacial Electrochem.*, 1989, **267**, 207–220.
43 F. P. A. Johnson, M. W. George, F. Hartl and J. J. Turner, *Organometallics*, 1996, **15**, 3374–3387.
44 D. R. Kauffman, D. Alfonso, C. Matranga, H. Qian and R. Jin, *J. Am. Chem. Soc.*, 2012, **134**, 10237–10243.
45 G. K. Ramesha, J. F. Brennecke and P. V. Kamat, *ACS Catal.*, 2014, **4**, 3249–3254.
46 G. J. Stor, F. Hartl, J. W. M. van Outersterp and D. J. Stufkens, *Organometallics*, 1995, **14**, 1115–1131.
47 S. Berger, A. Klein, W. Kaim and J. Fiedler, *Inorg. Chem.*, 1998, **37**, 5664–5671.
48 S. R. Batten, N. R. Champness, X.-M. Chen, J. Garcia-Martinez, S. Kitagawa, L. Öhrström, M. O'Keeffe, M. Paik Suh and J. Reedijk, *Pure Appl. Chem.*, 2013, **85**, 1715.
49 B. F. Hoskins and R. Robson, *J. Am. Chem. Soc.*, 1989, **111**, 5962–5964.
50 A. Schneemann, S. Henke, I. Schwedler and R. A. Fischer, *ChemPhysChem*, 2014, **15**, 823–839.
51 M. Eddaoudi, J. Kim, N. Rosi, D. Vodak, J. Wachter, M. O'Keeffe and O. M. Yaghi, *Science*, 2002, **295**, 469–472.
52 C. G. Freyschlag and R. J. Madix, *Mater. Today*, 2011, **14**, 134–142.
53 R. Robson, *J. Chem. Soc., Dalton Trans.*, 2000, 3735–3744, DOI: 10.1039/B003591M.
54 W. Xia, A. Mahmood, R. Zou and Q. Xu, *Energy Environ. Sci.*, 2015, **8**, 1837–1866.
55 X.-F. Lu, P.-Q. Liao, J.-W. Wang, J.-X. Wu, X.-W. Chen, C.-T. He, J.-P. Zhang, G.-R. Li and X.-M. Chen, *J. Am. Chem. Soc.*, 2016, **138**, 8336–8339.
56 S. R. Vaddipalli, S. R. Sanivarapu, S. Vengatesan, J. B. Lawrence, M. Eashwar and G. Sreedhar, *ACS Appl. Mater. Interfaces*, 2016, **8**, 23049–23059.

57 A.-Y. Lu, X. Yang, C.-C. Tseng, S. Min, S.-H. Lin, C.-L. Hsu, H. Li, H. Idriss, J.-L. Kuo, K.-W. Huang and L.-J. Li, *Small*, 2016, **12**, 5530–5537.
58 X. Hu and S. Dong, *J. Mater. Chem.*, 2008, **18**, 1279–1295.
59 C. Jin, J. Zhu, R. Dong, Z. Chen and Q. Huo, *Int. J. Hydrogen Energy*, 2016, **41**, 16851–16857.
60 J. Zhang, H. Li, P. Guo, H. Ma and X. S. Zhao, *J. Mater. Chem. A*, 2016, **4**, 8497–8511.
61 T. N. Pham-Truong, F. Lafolet, J. Ghilane and H. Randriamahazaka, *Electrochem. Commun.*, 2016, **70**, 13–17.
62 T. D. Gladysheva, B. I. Podlovchenko, D. S. Volkov and A. Y. Filatov, *Mendeleev Commun.*, 2016, **26**, 298–300.
63 S. Zhu and M. Shao, *J. Solid State Chem.*, 2016, **20**, 861–873.
64 J. Xiao, Q. Kuang, S. Yang, F. Xiao, S. Wang and L. Guo, *Sci. Rep.*, 2013, **3**, 2300.
65 S. Oh, J. R. Gallagher, J. T. Miller and Y. Surendranath, *J. Am. Chem. Soc.*, 2016, **138**, 1820–1823.
66 I. Hod, W. Bury, D. M. Karlin, P. Deria, C. W. Kung, M. J. Katz, M. So, B. Klahr, D. Jin, Y. W. Chung, T. W. Odom, O. K. Farha and J. T. Hupp, *Adv. Mater.*, 2014, **26**, 6295–6300.
67 Y. Zhao, N. Kornienko, Z. Liu, C. Zhu, S. Asahina, T.-R. Kuo, W. Bao, C. Xie, A. Hexemer, O. Terasaki, P. Yang and O. M. Yaghi, *J. Am. Chem. Soc.*, 2015, **137**, 2199–2202.
68 S. Homayoonnia and S. Zeinali, *Sens. Actuators, B*, 2016, **237**, 776–786.
69 S. Hermes, F. Schröder, R. Chelmowski, C. Wöll and R. A. Fischer, *J. Am. Chem. Soc.*, 2005, **127**, 13744–13745.
70 N. Mohaghegh, M. Tasviri, E. Rahimi and M. R. Gholami, *Appl. Surf. Sci.*, 2015, **351**, 216–224.
71 C. Wang, Z. Xie, K. E. deKrafft and W. Lin, *J. Am. Chem. Soc.*, 2011, **133**, 13445–13454.
72 L. Li, S. Zhang, L. Xu, J. Wang, L.-X. Shi, Z.-N. Chen, M. Hong and J. Luo, *Chem. Sci.*, 2014, **5**, 3808–3813.
73 W. Liang, T. L. Church, S. Zheng, C. Zhou, B. S. Haynes and D. M. D'Alessandro, *Chem. – Eur. J.*, 2015, **21**, 18576–18579.
74 A. Mahmood, W. Guo, H. Tabassum and R. Zou, *Adv. Energy Mater.*, 2016, **6**, 16000423, DOI: 10.1002/aenm.201600423.
75 S. Ma, G. A. Goenaga, A. V. Call and D. J. Liu, *Chem. – Eur. J.*, 2011, **17**, 2063–2067.
76 N. J. English, M. M. El-Hendawy, D. A. Mooney and J. M. D. MacElroy, *Coord. Chem. Rev.*, 2014, **269**, 85–95.
77 K. Ogura, H. Sugihara, J. Yano and M. Higasa, *J. Electrochem. Soc.*, 1994, **141**, 419–424.
78 Q. Lu, J. Rosen, Y. Zhou, G. S. Hutchings, Y. C. Kimmel, J. G. Chen and F. Jiao, *Nat. Commun.*, 2014, **5**, 3242.
79 B. Kumar, J. P. Brian, V. Atla, S. Kumari, K. A. Bertram, R. T. White and J. M. Spurgeon, *Catal. Today*, 2016, **270**, 19–30.
80 C. Amatore and J. M. Saveant, *J. Am. Chem. Soc.*, 1981, **103**, 5021–5023.
81 R. Schrebler, P. Cury, F. Herrera, H. Gómez and R. Córdova, *J. Electroanal. Chem.*, 2001, **516**, 23–30.
82 Y. Chen and M. W. Kanan, *J. Am. Chem. Soc.*, 2012, **134**, 1986–1989.
83 F. Fischer and H. Tropsch, *Ber. Dtsch. Chem. Ges.*, 1927, **60**, 1330–1334.
84 A. Schönweiz, J. Debuschewitz, S. Walter, R. Wölfel, H. Hahn, K. M. Dyballa, R. Franke, M. Haumann and P. Wasserscheid, *ChemCatChem*, 2013, **5**, 2955–2963.
85 G. Hayward and S. Baksa, *Anal. Methods*, 2013, **5**, 1708–1714.
86 I. C. Um and Y. H. Park, *Fibers Polym.*, 2007, **8**, 579–585.
87 K. W. Frese, *J. Electrochem. Soc.*, 1991, **138**, 3338–3344.
88 Y. Hori, R. Takahashi, Y. Yoshinami and A. Murata, *J. Phys. Chem. B*, 1997, **101**, 7075–7081.
89 J. Lee and Y. Tak, *Electrochim. Acta*, 2001, **46**, 3015–3022.
90 M. Gattrell, N. Gupta and A. Co, *J. Electroanal. Chem.*, 2006, **594**, 1–19.
91 X. Nie, M. R. Esopi, M. J. Janik and A. Asthagiri, *Angew. Chem., Int. Ed.*, 2013, **52**, 2459–2462.
92 C. W. Li and M. W. Kanan, *J. Am. Chem. Soc.*, 2012, **134**, 7231–7234.
93 M. Le, M. Ren, Z. Zhang, P. T. Sprunger, R. L. Kurtz and J. C. Flake, *J. Electrochem. Soc.*, 2011, **158**, E45–E49.
94 R. Hinogami, S. Yotsuhashi, M. Deguchi, Y. Zenitani, H. Hashiba and Y. Yamada, *ECS Electrochem. Lett.*, 2012, **1**, H17–H19.
95 R. S. Kumar, S. S. Kumar and M. A. Kulandainathan, *Electrochem. Commun.*, 2012, **25**, 70–73.
96 J. Albo, D. Vallejo, G. Beobide, O. Castillo, P. Castaño and A. Irabien, *ChemSusChem*, 2016, DOI: 10.1002/cssc.201600693.
97 J. Albo and A. Irabien, *J. Catal.*, 2016, **343**, 232–239.
98 L. Huang, H. Wang, J. Chen, Z. Wang, J. Sun, D. Zhao and Y. Yan, *Microporous Mesoporous Mater.*, 2003, **58**, 105–114.
99 D. Ren, Y. Deng, A. D. Handoko, C. S. Chen, S. Malkhandi and B. S. Yeo, *ACS Catal.*, 2015, **5**, 2814–2821.
100 H. Yoshio, K. Katsuhei, M. Akira and S. Shin, *Chem. Lett.*, 1986, **15**, 897–898.
101 D. W. DeWulf, T. Jin and A. J. Bard, *J. Electrochem. Soc.*, 1989, **136**, 1686–1691.
102 K. Hara, A. Tsuneto, A. Kudo and T. Sakata, *J. Electrochem. Soc.*, 1994, **141**, 2097–2103.
103 E. A. Mohamed, Z. N. Zahran and Y. Naruta, *Chem. Commun.*, 2015, **51**, 16900–16903.
104 D. Quezada, J. Honores, M. Garcia, F. Armijo and M. Isaacs, *New J. Chem.*, 2014, **38**, 3606–3612.
105 J. Choi, T. M. Benedetti, R. Jalili, A. Walker, G. G. Wallace and D. L. Officer, *Chem. – Eur. J.*, 2016, **22**, 14158–14161.
106 B. Mondal, A. Rana, P. Sen and A. Dey, *J. Am. Chem. Soc.*, 2015, **137**, 11214–11217.
107 R. B. Ambre, Q. Daniel, T. Fan, H. Chen, B. Zhang, L. Wang, M. S. G. Ahlquist, L. Duan and L. Sun, *Chem. Commun.*, 2016, **52**, 14478–14481.
108 J. E. Pander, A. Fogg and A. B. Bocarsly, *ChemCatChem*, 2016, **8**, 3536–3545.
109 S. Lin, C. S. Diercks, Y. B. Zhang, N. Kornienko, E. M. Nichols, Y. Zhao, A. R. Paris, D. Kim, P. Yang, O. M. Yaghi and C. J. Chang, *Science*, 2015, **349**, 1208–1213.

110 N. Kornienko, Y. Zhao, C. S. Kley, C. Zhu, D. Kim, S. Lin, C. J. Chang, O. M. Yaghi and P. Yang, *J. Am. Chem. Soc.*, 2015, **137**, 14129–14135.
111 A. Drygała, L. A. Dobrzański, M. Szindler, M. M. Szindler, M. Prokopiuk vel Prokopowicz and E. Jonda, *Int. J. Hydrogen Energy*, 2016, **41**, 7563–7567.
112 C. G. Carvajal, S. Rout, R. Mundle and A. K. Pradhan, *Langmuir*, 2017, **33**, 11–18.
113 I. Hod, M. D. Sampson, P. Deria, C. P. Kubiak, O. K. Farha and J. T. Hupp, *ACS Catal.*, 2015, **5**, 6302–6309.
114 J. Bonin, M. Robert and M. Routier, *J. Am. Chem. Soc.*, 2014, **136**, 16768–16771.
115 C. Costentin, S. Drouet, G. Passard, M. Robert and J.-M. Savéant, *J. Am. Chem. Soc.*, 2013, **135**, 9023–9031.
116 C. W. Machan, M. D. Sampson, S. A. Chabolla, T. Dang and C. P. Kubiak, *Organometallics*, 2014, **33**, 4550–4559.
117 C. Riplinger and E. A. Carter, *ACS Catal.*, 2015, **5**, 900–908.
118 C. W. Machan and C. P. Kubiak, *Dalton Trans.*, 2016, **45**, 15942–15950, DOI: 10.1039/C6DT01956K.
119 C. Riplinger, M. D. Sampson, A. M. Ritzmann, C. P. Kubiak and E. A. Carter, *J. Am. Chem. Soc.*, 2014, **136**, 16285–16298.
120 J. M. Smieja and C. P. Kubiak, *Inorg. Chem.*, 2010, **49**, 9283–9289.
121 L. Ye, J. X. Liu, Y. Gao, C. H. Gong, M. Addicoat, T. Heine, C. Woll and L. C. Sun, *J. Mater. Chem. A*, 2016, **4**, 15320–15326.
122 M. C. So, S. Jin, H.-J. Son, G. P. Wiederrecht, O. K. Farha and J. T. Hupp, *J. Am. Chem. Soc.*, 2013, **135**, 15698–15701.
123 O. Shekhah, J. Liu, R. A. Fischer and C. Woll, *Chem. Soc. Rev.*, 2011, **40**, 1081–1106.
124 X. Kang, Q. Zhu, X. Sun, J. Hu, J. Zhang, Z. Liu and B. Han, *Chem. Sci.*, 2016, **7**, 266–273.
125 B. M. Hunter, H. B. Gray and A. M. Müller, *Chem. Rev.*, 2016, **116**, 14120–14136.
126 D. Merki and X. Hu, *Energy Environ. Sci.*, 2011, **4**, 3878–3888.
127 S. Neudeck, S. Maji, I. López, S. Meyer, F. Meyer and A. Llobet, *J. Am. Chem. Soc.*, 2014, **136**, 24–27.
128 E. Tsuji, A. Imanishi, K.-I. Fukui and Y. Nakato, *Electrochim. Acta*, 2011, **56**, 2009–2016.
129 R. Lalrempuia, N. D. McDaniel, H. Müller-Bunz, S. Bernhard and M. Albrecht, *Angew. Chem., Int. Ed.*, 2010, **49**, 9765–9768.
130 S. W. Sheehan, J. M. Thomsen, U. Hintermair, R. H. Crabtree, G. W. Brudvig and C. A. Schmuttenmaer, *Nat. Commun.*, 2015, **6**, 6469.
131 A. Mills, *Chem. Soc. Rev.*, 1989, **18**, 285–316.
132 J. L. Fillol, Z. Codolà, I. Garcia-Bosch, L. Gómez, J. J. Pla and M. Costas, *Nat. Chem.*, 2011, **3**, 807–813.
133 Y. Han, Y. Wu, W. Lai and R. Cao, *Inorg. Chem.*, 2015, **54**, 5604–5613.
134 S. M. Barnett, K. I. Goldberg and J. M. Mayer, *Nat. Chem.*, 2012, **4**, 498–502.
135 F. Evangelisti, R. Güttinger, R. Moré, S. Luber and G. R. Patzke, *J. Am. Chem. Soc.*, 2013, **135**, 18734–18737.
136 M. Al-Mamun, Y. Wang, P. Liu, Y. L. Zhong, H. Yin, X. Su, H. Zhang, H. Yang, D. Wang, Z. Tang and H. Zhao, *J. Mater. Chem. A*, 2016, **4**, 18314–18321.
137 S. Pintado, S. Goberna-Ferrón, E. C. Escudero-Adán and J. R. Galán-Mascarós, *J. Am. Chem. Soc.*, 2013, **135**, 13270–13273.
138 J. Rossmeisl, Z. W. Qu, H. Zhu, G. J. Kroes and J. K. Nørskov, *J. Electroanal. Chem.*, 2007, **607**, 83–89.
139 T. Shinagawa, A. T. Garcia-Esparza and K. Takanabe, *Sci. Rep.*, 2015, **5**, 13801.
140 J. J. Low, A. I. Benin, P. Jakubczak, J. F. Abrahamian, S. A. Faheem and R. R. Willis, *J. Am. Chem. Soc.*, 2009, **131**, 15834–15842.
141 Y. Gong, H.-F. Shi, Z. Hao, J.-L. Sun and J.-H. Lin, *Dalton Trans.*, 2013, **42**, 12252–12259.
142 M. W. Kanan, Y. Surendranath and D. G. Nocera, *Chem. Soc. Rev.*, 2009, **38**, 109–114.
143 M. W. Kanan and D. G. Nocera, *Science*, 2008, **321**, 1072–1075.
144 J. B. Gerken, J. G. McAlpin, J. Y. C. Chen, M. L. Rigsby, W. H. Casey, R. D. Britt and S. S. Stahl, *J. Am. Chem. Soc.*, 2011, **133**, 14431–14442.
145 J. Chen and A. Selloni, *J. Phys. Chem. Lett.*, 2012, **3**, 2808–2814.
146 F. Jiao and H. Frei, *Angew. Chem., Int. Ed.*, 2009, **48**, 1841–1844.
147 K. S. Park, Z. Ni, A. P. Côté, J. Y. Choi, R. Huang, F. J. Uribe-Romo, H. K. Chae, M. O'Keeffe and O. M. Yaghi, *Proc. Natl. Acad. Sci. U. S. A.*, 2006, **103**, 10186–10191.
148 S. Wang, Y. Hou, S. Lin and X. Wang, *Nanoscale*, 2014, **6**, 9930–9934.
149 F. Dai, W. Fan, J. Bi, P. Jiang, D. Liu, X. Zhang, H. Lin, C. Gong, R. Wang, L. Zhang and D. Sun, *Dalton Trans.*, 2016, **45**, 61–65.
150 P. M. Usov, S. R. Ahrenholtz, W. A. Maza, B. Stratakes, C. C. Epley, M. C. Kessinger, J. Zhu and A. J. Morris, *J. Mater. Chem. A*, 2016, **4**, 16818–16823.
151 L. Wang, Y. Wu, R. Cao, L. Ren, M. Chen, X. Feng, J. Zhou and B. Wang, *ACS Appl. Mater. Interfaces*, 2016, **8**, 16736–16743.
152 K. F. Babu, M. A. Kulandainathan, I. Katsounaros, L. Rassaei, A. D. Burrows, P. R. Raithby and F. Marken, *Electrochem. Commun.*, 2010, **12**, 632–635.
153 D. Strmcnik, P. P. Lopes, B. Genorio, V. R. Stamenkovic and N. M. Markovic, *Nano Energy*, 2016, **29**, 29–36.
154 W. Zhang, W. Lai and R. Cao, *Chem. Rev.*, 2017, **117**, 3717–3797, DOI: 10.1021/acs.chemrev.6b00299.
155 P. C. K. Vesborg, B. Seger and I. Chorkendorff, *J. Phys. Chem. Lett.*, 2015, **6**, 951–957.
156 S. Fletcher, *J. Solid State Chem.*, 2009, **13**, 537–549.
157 Y. Gong, H.-F. Shi, P.-G. Jiang, W. Hua and J.-H. Lin, *Cryst. Growth Des.*, 2014, **14**, 649–657.
158 Y. Gong, Z. Hao, J. Meng, H. Shi, P. Jiang, M. Zhang and J. Lin, *ChemPlusChem*, 2014, **79**, 266–277.
159 B. Keita and L. Nadjo, *J. Mol. Catal. A: Chem.*, 2007, **262**, 190–215.

160 R. Liu, S. Li, G. Zhang, A. Dolbecq, P. Mialane and B. Keita, *J. Cluster Sci.*, 2014, **25**, 711–740.
161 Y. Gong, T. Wu, P. G. Jiang, J. H. Lin and Y. X. Yang, *Inorg. Chem.*, 2013, **52**, 777–784.
162 D.-Y. Du, J.-S. Qin, S.-L. Li, Z.-M. Su and Y.-Q. Lan, *Chem. Soc. Rev.*, 2014, **43**, 4615–4632.
163 B. Nohra, H. El Moll, L. M. Rodriguez Albelo, P. Mialane, J. Marrot, C. Mellot-Draznieks, M. O'Keeffe, R. Ngo Biboum, J. Lemaire, B. Keita, L. Nadjo and A. Dolbecq, *J. Am. Chem. Soc.*, 2011, **133**, 13363–13374.
164 G. Rousseau, L. M. Rodriguez-Albelo, W. Salomon, P. Mialane, J. Marrot, F. Doungmene, I.-M. Mbomekallé, P. de Oliveira and A. Dolbecq, *Cryst. Growth Des.*, 2015, **15**, 449–456.
165 L. Marleny Rodriguez-Albelo, A. R. Ruiz-Salvador, A. Sampieri, D. W. Lewis, A. Gómez, B. Nohra, P. Mialane, J. Marrot, F. Sécheresse, C. Mellot-Draznieks, R. Ngo Biboum, B. Keita, L. Nadjo and A. Dolbecq, *J. Am. Chem. Soc.*, 2009, **131**, 16078–16087.
166 J.-S. Qin, D.-Y. Du, W. Guan, X.-J. Bo, Y.-F. Li, L.-P. Guo, Z.-M. Su, Y.-Y. Wang, Y.-Q. Lan and H.-C. Zhou, *J. Am. Chem. Soc.*, 2015, **137**, 7169–7177.
167 M. Shao, Q. Chang, J.-P. Dodelet and R. Chenitz, *Chem. Rev.*, 2016, **116**, 3594–3657.
168 Y.-B. Huang, J. Liang, X.-S. Wang and R. Cao, *Chem. Soc. Rev.*, 2017, **46**, 126–157, DOI: 10.1039/C6CS00250A.
169 H. Zhang, H. Osgood, X. Xie, Y. Shao and G. Wu, *Nano Energy*, 2017, **31**, 331–350.
170 S. R. Ahrenholtz, C. C. Epley and A. J. Morris, *J. Am. Chem. Soc.*, 2014, **136**, 2464–2472.
171 T. Ishimoto, T. Ogura, M. Koyama, L. Yang, S. Kinoshita, T. Yamada, M. Tokunaga and H. Kitagawa, *J. Phys. Chem. C*, 2013, **117**, 10607–10614.
172 L. Yang, S. Kinoshita, T. Yamada, S. Kanda, H. Kitagawa, M. Tokunaga, T. Ishimoto, T. Ogura, R. Nagumo, A. Miyamoto and M. Koyama, *Angew. Chem., Int. Ed.*, 2010, **49**, 5348–5351.
173 A. Vulcu, L. Olenic, G. Blanita and C. Berghian-Grosan, *Electrochim. Acta*, 2016, **219**, 630–637.
174 G. Jia, Y. Gao, W. Zhang, H. Wang, Z. Cao, C. Li and J. Liu, *Electrochem. Commun.*, 2013, **34**, 211–214.
175 Y. Zhang, X. Bo, A. Nsabimana, C. Han, M. Li and L. Guo, *J. Mater. Chem. A*, 2015, **3**, 732–738.
176 C.-W. Kung, T.-H. Chang, L.-Y. Chou, J. T. Hupp, O. K. Farha and K.-C. Ho, *Electrochem. Commun.*, 2015, **58**, 51–56.
177 C. Zhang, M. Wang, L. Liu, X. Yang and X. Xu, *Electrochem. Commun.*, 2013, **33**, 131–134.
178 Y. Li, C. Huangfu, H. Du, W. Liu, Y. Li and J. Ye, *J. Electroanal. Chem.*, 2013, **709**, 65–69.
179 A. S. Lytvynenko, R. A. Polunin, M. A. Kiskin, A. M. Mishura, V. E. Titov, S. V. Kolotilov, V. M. Novotortsev and I. L. Eremenko, *Theor. Exp. Chem.*, 2015, **51**, 54–61.
180 B.-X. Dong, L. Chen, S.-Y. Zhang, J. Ge, L. Song, H. Tian, Y.-L. Teng and W.-L. Liu, *Dalton Trans.*, 2015, **44**, 1435–1440.
181 N. C. Burtch, H. Jasuja and K. S. Walton, *Chem. Rev.*, 2014, **114**, 10575–10612.
182 F. Afsahi and S. Kaliaguine, *J. Mater. Chem. A*, 2014, **2**, 12270–12279.
183 B. Volosskiy, H. Fei, Z. Zhao, S. Lee, M. Li, Z. Lin, B. Papandrea, C. Wang, Y. Huang and X. Duan, *ACS Appl. Mater. Interfaces*, 2016, **8**, 26769–26774.
184 P. M. Usov, C. McDonnell-Worth, F. Zhou, D. R. MacFarlane and D. M. D'Alessandro, *Electrochim. Acta*, 2015, **153**, 433–438.
185 Z. Zhang, H. T. H. Nguyen, S. A. Miller, A. M. Ploskonka, J. B. DeCoste and S. M. Cohen, *J. Am. Chem. Soc.*, 2016, **138**, 920–925.
186 Z. Zhang, H. T. H. Nguyen, S. A. Miller and S. M. Cohen, *Angew. Chem., Int. Ed.*, 2015, **54**, 6152–6157.
187 L. Sun, M. G. Campbell and M. Dincă, *Angew. Chem., Int. Ed.*, 2016, **55**, 3566–3579.
188 C. F. Leong, P. M. Usov and D. M. D'Alessandro, *MRS Bull.*, 2016, **41**, 858–864.
189 D. M. D'Alessandro, J. R. R. Kanga and J. S. Caddy, *Aust. J. Chem.*, 2011, **64**, 718–722.
190 C. H. Su, C. W. Kung, T. H. Chang, H. C. Lu, K. C. Ho and Y. C. Liao, *J. Mater. Chem. A*, 2016, **4**, 11094–11102.